Mineral dust aerosol impacts on global climate and climate change

Jasper F. Kok[1, †], Trude Storelvmo[2], Vlassis A. Karydis[3], Adeyemi A. Adebiyi[4], Natalie M. Mahowald[5], Amato T. Evan[6], Cenlin He[7] and Danny M. Leung[1]

[1]*Department of Atmospheric and Oceanic Sciences, University of California - Los Angeles, Los Angeles, CA, USA*
[2]*Department of Geoscience, University of Oslo, Oslo, Norway*
[3]*Institute for Energy and Climate Research: Troposphere, Forschungszentrum Jülich GmbH, Jülich, Germany*
[4]*Department of Life and Environmental Sciences, University of California - Merced, Merced, USA*
[5]*Department of Earth and Atmospheric Sciences, Cornell University, Ithaca, NY, USA*
[6]*Scripps Institution of Oceanography, University of California, San Diego, CA, USA*
[7]*Research Applications Laboratory, National Center for Atmospheric Research, Boulder, CO, USA*
[†]*Corresponding author: jfkok@ucla.edu*

This is the manuscript version before editorial editing and typesetting. The final article was published as:

This paper was published as Kok, J.F., Storelvmo, T., Karydis, V.A., Adebiyi, A.A., Mahowald, N.M., Evan, A.T., He, C., and Leung, D.M., Mineral dust aerosol impacts on global climate and climate change. *Nat Rev Earth Environ*, 4, 71-86 (2023), https://doi.org/10.1038/s43017-022-00379-5

Abstract

Mineral dust aerosols impact Earth's energy budget through interactions with radiation, clouds, atmospheric chemistry, the cryosphere and biogeochemistry. In this review, we summarize these interactions and assess the resulting impacts of dust, and of changes in dust, on global climate and climate change. We find that the total effect of these interactions on Earth's global energy budget—the dust effective radiative effect—is -0.2 ± 0.5 Wm^{-2} (90% confidence interval). Compared to pre-industrial times, global dust mass loading is 55 ± 30% higher in the modern climate, leading to changes in the Earth's energy budget. Indeed, this increase in dust has produced a global mean effective radiative forcing of -0.07 ± 0.18 Wm^{-2}. Current climate models and climate assessments do not represent the historical increase in dust and thus omit the resulting radiative forcing, biasing climate change projections and assessments of climate sensitivity. Climate model simulations of future changes in dust diverge widely and are very uncertain. Further work is thus needed to constrain the radiative effects of dust on climate and to improve the representation of dust in climate models.

Key points

1. The direct radiative effect due to dust interactions with radiation is -0.15 ± 0.35 Wm^{-2} and accounts for a large fraction of the dust effective radiative effect and its uncertainty.
2. Dust interactions with clouds, atmospheric chemistry, the cryosphere, and biogeochemistry also contribute considerably to the uncertainty in the dust effective radiative effect, in part because of a lack of observational constraints, which are urgently needed.
3. Dust mass loading generated by all major source regions has increased since pre-industrial times, namely by 46 (2-102) % for North African dust, by 74 ± 37 % for Asian dust, and by 27 (-14 to 88) % for Southern Hemisphere dust.
4. It is more likely that dust net cools than that it net warms global climate.
5. The historical increase in dust has likely somewhat counteracted greenhouse warming.
6. Careful simulations with coupled climate models that reproduce the historical dust increase are needed to better constrain dust radiative forcing.

Introduction

Mineral dust aerosols are small rock-derived particles with diameter D <~100 μm that are suspended in the atmosphere[1,2]. Most dust is produced by the ballistic impacts of wind-driven sand grains on sparsely vegetated and dry soils[3], which ejects and fragments aggregates of soil particles[1,4]. Owing to these mechanical impacts, dust is a relatively coarse aerosol, with most of its mass contained in the coarse (D > 2.5 μm) and super coarse (D > 10 μm) modes[5].

Dust is produced in copious amounts in the world's deserts, loading the atmosphere with ~26 million tonnes of dust, which accounts for a large majority of the atmosphere's aerosol burden by mass[6,7]. The Sahara Desert and the Sahel contribute ~50% of global dust emissions (~2100 Tg/yr) and mass loading (~13 Tg), the Asian deserts ~40% (~2000 Tg/yr and ~10 Tg), and the North American and Southern Hemisphere deserts and high latitude regions another ~10% (~500 Tg/yr and ~3 Tg) (**Fig. 1**)[8,9]. Although much of the dust is deposited close to source regions, a substantial fraction is transported for thousands of kilometres. For example, plumes of African dust regularly travel across the tropical North Atlantic, reaching the southwestern United States and the Amazon Basin[10].

The abundance and long-range transport of dust cause it to impact climate through various mechanisms. During transport, dust scatters and absorbs solar shortwave (SW) and terrestrial longwave (LW) radiation[6,11], modifies cloud properties through seeding cloud droplets and ice crystals[12,13], mixes with other aerosols[14], and serves as a sink for radiatively important atmospheric trace gases[14-17]. Upon deposition, dust darkens snow and ice packs[18,19], and stimulates ecosystem productivity and CO_2 drawdown through the delivery of iron and phosphorus[20]. Because some of these mechanisms cool whereas others warm[6,14,21], it is unclear whether dust exerts a net cooling or a net warming effect on global climate. Because measurements of dust deposition suggest that dust has increased since the pre-industrial era[22,23], this uncertainty in the sign and magnitude of dust radiative effects means it is unknown whether dust changes have enhanced or opposed anthropogenic warming.

In this review, we examine the impacts of dust, and of changes in dust, on global climate and climate change. We first summarize the various mechanisms through which dust impacts Earth's radiation budget, and assess the radiative effect produced by each mechanism. We then constrain the increase in dust loading since pre-industrial times and assess the radiative perturbation produced by this historical increase in dust. We also discuss the radiative perturbation due to possible future changes in dust and end with recommendations for future research priorities.

Mechanisms by which dust impacts climate

Dust can perturb Earth's energy balance via various mechanisms. In each case, a radiative effect arises, defined as the imbalance between incoming net solar radiation and outgoing infrared radiation at the top-of-atmosphere (TOA) resulting from an atmospheric constituent (in this case, dust)[24]. These effects can be either instantaneous, such as scattering and absorbing SW and LW radiation, or an adjustment, such as altering cloud cover[25].

We calculate the radiative effect due to mechanism i in the modern climate, $\boldsymbol{r_i}$ ($\mathrm{Wm^{-2}}$), as the change in Earth's energy balance, $\boldsymbol{\Delta f}_i$ ($\mathrm{Wm^{-2}}$), produced per change in global dust mass loading from modern levels, $\boldsymbol{\Delta L_i}$ (Tg), multiplied by the global modern dust loading, L (Tg). That is,

$$r_i \equiv \frac{\Delta f_i}{\Delta L_i} L. \tag{1}$$

The sum of all radiative effects then equals the effective radiative effect of dust, $\boldsymbol{R}$ ($\mathrm{Wm^{-2}}$), which includes both instantaneous radiative effects and adjustments[25,27],

$$R = \sum_i r_i. \tag{2}$$

Eqs. (1) and (2) define the dust effective radiative effect in such a way that it can be used to obtain the radiative perturbation, $\boldsymbol{\Delta}F$, due to a change in dust loading, $\boldsymbol{\Delta L_{\mathrm{m}}}$, from its value in the modern climate,

$$\Delta F = R \frac{\Delta L_{\mathrm{m}}}{L}. \tag{3}$$

We then define the effective radiative forcing of dust due to the change $\boldsymbol{\Delta L_{\mathrm{p}\to\mathrm{m}}}$ in dust mass loading from pre-industrial to modern times as

$$\Delta F_{\mathrm{p}\to\mathrm{m}} = R \frac{\Delta L_{\mathrm{p}\to\mathrm{m}}}{L}. \tag{4}$$

Our use here of the term radiative forcing deviates slightly from previous work[25,27] in which it denotes radiative perturbations that are entirely from anthropogenic forcing agents. However, because dust is a natural aerosol affected by climate changes and human land use changes, a radiative perturbation due to a historical change in dust can be partially due to both human land use changes (a forcing) and natural and anthropogenic climate changes (a feedback). Because these two contributions are difficult to disentangle, we refer to the entire radiative perturbation due to the historical change in dust as the **dust** effective radiative forcing.

Radiative effects from dust arise through interactions with radiation, atmospheric chemistry, clouds, the cryosphere, and biogeochemistry (**Fig. 2**). Each of these mechanisms are now discussed.

Interactions with radiation

Perhaps the best understood mechanism by which dust impacts climate is through the dust direct radiative effect (DRE), the perturbation of Earth's energy balance by scattering and absorption of radiation (**Fig. 2a**). Since dust spans a wide range of sizes, from ~0.1 – 100 μm[29], it interacts with both SW (centered around 550 nm wavelength) and LW (centered around 10 μm wavelength) radiation[30,31].

The sign and magnitude of the dust DRE depend on the balance between these interactions. For instance, scattering of SW radiation cools the climate while absorption of SW radiation warms, with an overall net cooling[6,32]. In contrast, scattering and absorption of LW radiation both warm the climate since both decrease the transparency of the atmosphere to terrestrial LW radiation[33]. Thus, the balance between cooling from SW scattering, and warming from SW absorption and LW scattering and absorption, dictate the dust DRE.

For SW radiation, the balance between scattering and absorption is influenced by dust particle size. Because absorption increases more strongly with particle size than scattering[34,35], the single-scattering albedo (SSA; the ratio of scattered radiation to total extinguished radiation) decreases with particle size. Indeed, submicron dust has an SSA close to 1, whereas supermicron dust absorbs a substantial fraction of extinguished radiation, exhibiting SSAs of ~0.95 at D = 2 μm, ~0.80 at D = 10 μm, and even lower for super coarse dust[30,36].

However, the exact SSA of dust aerosols depends on their complex refractive index, determined by particle mineralogy[31]. Absorption increases approximately linearly with iron oxide content, which is primarily provided by hematite and goethite[37]. Dust optical properties can also be affected by mixing with other aerosols, especially black carbon[38]. Observations suggest that this possible mixing has limited impact on the optical properties of most African dust[39,40], but could substantially affect those of East Asian dust[41].

Although dust particle size and mineralogy determine the balance between SW scattering and absorption, the efficiency with which both processes perturb the TOA radiative flux depends on the albedo of the underlying surface. Indeed, the cooling effect of SW scattering is enhanced if the dust is situated above dark (low albedo) surfaces like the ocean and forests that would otherwise absorb most of the radiation[42]. Conversely, the warming effect of SW absorption is enhanced if the dust is situated above clouds or above high albedo land surfaces like snow, ice, and deserts that would otherwise scatter most of the radiation back to space[35,43].

Dust microphysical properties and mineralogy also influence the extinction of LW radiation. For example, because of its longer wavelengths, LW radiation is extinguished primarily by coarse dust[30,33,44]. The sensitivity of LW extinction to mineralogy is less important than for SW interactions owing to the smaller variability in LW optical properties between minerals, and because LW scattering and absorption both warm the planet[31,45,46].

The efficiency with which dust extinction of LW radiation perturbs the TOA radiative flux also depends on the atmosphere's transparency to LW radiation and the elevation of the dust layer. Indeed, the TOA flux is only substantially impacted if the atmosphere is at least somewhat transparent to LW radiation, as is the case in the absence of clouds in the ~8 – 13 μm 'atmospheric window' wavelength range[33,47]. Furthermore, because LW emission depends on temperature, the LW warming depends on the temperature difference between the dust layer and the source of the LW radiation - usually the surface or clouds below the dust layer. In addition, the atmosphere's transparency to LW radiation decreases with the concentration of water vapor

and thus increases with height. As such, dust warming by LW extinction increases approximately linearly with the height of the dust layer[33,42,47,48].

Although the processes by which dust interacts with SW and LW radiation are relatively well understood, the resulting radiative effects are poorly constrained. For dust interactions with SW radiation, central estimates of SW DRE are -0.40 Wm^{-2} (-0.10 to -0.70 Wm^{-2}, 90% confidence interval)[6,32,49-53] (**Fig. 3**); these estimates are determined using less absorbing optical properties and a coarser dust size distribution, consistent with experimental constraints[4,6,29,37,40,54-56]. The wide range reflects substantial uncertainties in the dust size distribution[6] and dust optical properties[46]. For dust interactions with LW radiation, best estimates of LW DRE are +0.25 Wm^{-2} with a range of +0.10 to +0.40 Wm^{-2} (**Fig. 3**) [6,32,46,49-52]; these estimates use realistic optical properties[45] and size distributions that are consistent with satellite constraints on the LW direct radiative effect[48,57]. The range reflects uncertainties in dust LW optical properties[45], the height of dust plumes[58,59], the dust size distribution and the contribution of super coarse dust[36,49,54], and the effect of LW scattering by dust, which is neglected in climate models[32,33] and is sometimes accounted for using a simple correction factor[6,32,46,52].

As a result of the uncertainties and opposing SW and LW DRE , it is unclear whether the dust DRE exerts a net cooling or warming effect. Combining the SW and LW DRE yields a net dust DRE of -0.15 ± 0.35 Wm^{-2}, consistent with other calculations [6,32,46,49-51] (**Fig. 3**). As such, the dust DRE could either slightly warm or substantially cool the planet, or it could have little net impact. We assign medium confidence to this assessment because of the large body of research and availability of satellite-based constraints.

Interactions with atmospheric chemistry

Dust affects atmospheric chemistry through numerous interactions with atmospheric trace gases and aerosols. Although freshly emitted mineral dust is considered insoluble, it is reactive towards trace acidic gases derived from anthropogenic pollutants and sea salt[17,60]. Mineral dust particles collected throughout the world are notably associated with nitrate[61-63]. Nitric acid interacts with the non-volatile mineral cations of dust, forming salts to maintain the charge balance in the aerosol phase[64]. The uptake of such acidic vapors is very rapid due to their ability to react with carbonates and other minerals through simple acid-base chemistry[65]. Over continents, such interactions of mineral cations with anthropogenic sulfuric acid causes the accumulation of substantial amounts of sulfate on dust surfaces[66]. In contrast, over oceans, mineral cations are commonly associated with chloride derived from sea salt[67].

Mineral dust also provides surfaces for the adsorption of inorganic (notably SO_2, NO_2, and O_3) and organic trace gases[17], affecting the optical properties, hygroscopicity and atmospheric residence time of both dust and anthropogenic aerosols. Therefore, dust particles provide a substantial sink for the direct removal of important atmospheric constituents like O_3, affecting the oxidative capacity of the atmosphere and the ozone radiative forcing[68,69]. Dust particles also provide reaction sites for the oxidation of SO_2 to sulfuric acid[70] and the formation of nitrous acid through heterogeneous reactions of NO_2[71]. However, such heterogeneous formation of salts occurs at a much slower pace than through the direct uptake of acidic vapours since acid anhydrides (for example SO_2) do not initially contain any acidic protons[65]. Additionally, the high pH values found on the alkaline mineral particles can promote the formation of ammonium nitrate on their surface[72,73].

All these interactions of dust with atmospheric gases can transform the surface and even the bulk chemical composition of dust particles[74,75]. This chemical processing of dust is highly dependent on both the gas phase composition and on the dust chemical composition[64,76], which depends on the mineralogy of the source soil[77].

The chemical ageing of dust due to these various reactions creates a soluble coating that increases the dust particle's hydrophilicity, which in turn affects the residence time of dust and its interactions with clouds. For example, the interaction of a calcite-containing dust particle with nitric acid converts the insoluble calcium carbonate to the highly hygroscopic calcium nitrate[78]. The increased hygroscopicity of the chemically aged dust increases its water adsorption efficiency, making it grow more rapidly under humid conditions, thus causing it to form cloud droplets and extinguish radiation more efficiently. On the contrary, the increased water uptake by the large, aged dust particles can also deplete in-cloud supersaturation, thereby reducing the number of smaller anthropogenic particles that are activated and grow into cloud droplets[13]. Furthermore, chemical ageing of mineral dust can also reduce its ice nucleating ability[80].

These heterogeneous and multiphase reactions affect the atmospheric loading of both dust and non-dust aerosols. Nitrate formation associated with the mineral cations removes nitric acid from the gas phase, decreasing the formation of ammonium nitrate aerosols. Similarly, sulfate formation on dust decreases SO_2 abundance and thus the formation of sulfate aerosols. As such, dust can reduce the concentration of anthropogenic CCN both by adsorption of precursor gases and through coagulation with anthropogenic aerosols. Furthermore, the hygroscopic growth of aged dust can increase its scavenging and deposition rate, reducing its atmospheric residence time and loading[15,81]. However, modelling results suggest that these effects can enhance the total accumulation mode dust burden through a reduced loss by coagulation with coarse dust particles[15].

The physicochemical interactions of mineral dust with atmospheric composition can thus affect the direct and indirect radiative forcing of both dust and non-dust aerosols (Fig. 2b). These effects can be both negative or positive, depending on the region and the prevailing impacts of dust on the atmospheric aerosol loading and composition[15,16]. A net cooling effect of -0.05 Wm^{-2} has been calculated for the effect of dust on the total aerosol DRE[15], driven mostly by an enhanced burden of the accumulation mode dust aerosols and decreased absorption of SW radiation due to the modified aerosol composition of mineral dust. However, observations of dust during transport across the Atlantic and Mediterranean oceans indicate that the size distribution of dust with diameters less than 5 μm remains remarkably constant and that optical properties do not change appreciably[39,40,55]. Moreover, a critical effect of heterogeneous chemistry on dust surfaces is to reduce the atmospheric loading of anthropogenic aerosols, thereby decreasing their direct radiative cooling, resulting in a net warming of +0.12 to +0.20 Wm^{-2} [16,82,83]. Overall, the impact of dust interactions with atmospheric chemistry on the aerosol DRE is highly uncertain. The resulting radiative effect is assessed at 0.10 ± 0.15 Wm^{-2} to encompass the possibility of the slight cooling of -0.05 Wm^{-2} [15] as a lower bound and the larger warming found by others[16,82,83] as an upper bound. We assign very low confidence to this assessment.

Interactions with clouds

Dust particles influence clouds via multiple interactions, including changing the thermodynamic environment by absorbing SW and LW radiation and serving as cloud condensation nuclei (CCN) and ice-nucleating particles (INPs). Radiative perturbations produced by dust effects on

warm clouds, mixed-phase clouds, cirrus (ice) clouds, and by semi-direct effects are discussed next.

Dust indirect effects on warm clouds

There are three main pathways through which dust particles can affect warm clouds: first,

by increasing the concentration of CCN, as laboratory studies have shown that various types of (unprocessed) mineral dusts possess a modest ability to act as CCN[84,85], which is further enhanced by atmospheric processing (ageing) of dust[86]; , second, by reducing the concentration of non-dust CCN through coagulation and adsorption of precursor gasses; and third by acting as giant CCN, which can form cloud droplets at relatively low supersaturation and thus deplete water vapor to such an extent that overall cloud droplet formation is suppressed. The second and third pathways are both thought to reduce cloud droplet number concentrations (CDNC), and thus reduce cloud albedo and shorten cloud lifetimes.

Although some modelling results found that the pathways that decrease CDNC dominate (Fig. 2c, lower branch), amounting to a decrease of as much as -11% in the global mean CDNC[13], most other modelling has found that dust slightly increases the global mean CDNC abundance. These latter results thus suggest that the effect of dust acting as CCN dominates (Fig. 2c, upper branch), albeit with large differences in the magnitude of the dust-induced CDNC contribution[21,87,88]. As a CDNC increase is expected to increase cloud albedo and extend cloud lifetime through well-established mechanisms[28], a dust-induced increase in CDNC would have a net cooling effect (Fig. 2c, upper branch). For example, global simulations with the CAM5 model[21] resulted in a ~1% increase in CDNC for a 3-fold increase in dust emissions, and this CDNC increase in turn produced a negative forcing of -0.01 Wm^{-2}. Such an effect is indeed supported by estimates based on satellite observations[89].

Although past work thus reached contradictory conclusions regarding the net global effects of dust on warm clouds, there is broad agreement that the sign and magnitude of the dust contribution to CDNC is highly heterogeneous in both space and time[13,21]. Given the relatively sparse research and disagreement on the sign of the global mean CDNC contribution from dust, we assess the corresponding perturbation to Earth's TOA radiation budget through changes to liquid clouds to likely be negative but close to zero, with an uncertainty range of -0.10 to +0.10 Wm^{-2}. This assessment is based on scaling the estimates of CCN/CDNC changes[13,21,87,88] with the forcing estimate per change in CCN/CDNCcited above[21], and has low confidence.

Dust indirect effects on mixed-phase clouds

Although the ability of dust to act as CCN is somewhat ambiguous, their ice-nucleating ability is undisputed[90,91]. A wide variety of dust particles have been investigated in the laboratory and found to be efficient INPs both in the immersion mode (freezing cloud droplets from within) and in the deposition mode (nucleating ice through vapor depositing onto them, possibly triggered by freezing of condensed water in particle pores[92]). The former is the ice formation mechanism thought to be of greatest relevance for mixed-phase clouds (MPCs). These are clouds with temperatures between approximately -38°C and 0°C that can consist of either supercooled liquid droplets, ice crystals, or a mixture. MPCs are generally optically thick and efficiently reflect incoming SW radiation (a cooling effect). Their optical thickness also allows them to absorb virtually all outgoing LW radiation, reducing the amount of LW radiation emitted to space (a warming effect). The former (SW) effect has been found to dominate in the global mean[93]. In an

INP-limited ("pristine") environment, MPCs will be optically thick and usually have liquid cloud tops[94], with only small amounts of ice residing in the cloud interior or below cloud base as ice crystals rapidly grow and sediment out (Fig. 2d, left schematic). In a dust-enriched environment, MPCs will be partly or completely glaciated, depending on the dust abundance and INP efficiency. This cloud glaciation results in an overall reduction of cloud albedo and thus a positive (warming) radiative effect (Fig. 2d, right schematic). An increase in dust loading, and thus INPs, therefore likely produce a warming effect on climate by reducing the cooling effect of MPCs (Fig. 2d).

Modelling results on the effects of dust on MPCs generally agree qualitatively, but differ quantitatively. Global simulations with the E3SM model[95] found that dust effects on mixed-phase clouds perturb the TOA radiation budget by +0.05 to +0.26 Wm^{-2}. This perturbation arises from a reduction in cloud liquid water and a corresponding increase in cloud ice (Fig. 2d). For comparison, global simulations with the CAM5 model estimated that going from a very pristine state with only 10% of current dust emissions to present-day dust emissions induced a perturbation of only 0.01 to 0.10 Wm^{-2} through dust-INP effects on mixed-phase clouds, again by shifting cloud phase in favor of more ice[21]. However, as the atmospheric dust loading change in the latter study is smaller than in the former, these estimates are broadly consistent with each other. These modelling results are further supported by satellite observations that found that dust-enriched environments tend to have MPCs with a larger proportion of ice than their counterparts in largely dust-free environments[96,97]. Thus, a perturbation to the TOA radiation budget of approximately 0.10 Wm^{-2} due to dust effects on MPCs is supported, but with a relatively large assessed uncertainty range of 0 to 0.20 Wm^{-2} and low confidence, owing to the limited body of research.

Dust indirect effects on cirrus clouds

The dominant role of dust particles in cirrus cloud formation worldwide is supported by in situ measurements, satellite observations, and numerical modelling[98,99]. Cirrus clouds are pure ice clouds residing in the upper troposphere at temperatures below approximately -38°C. These clouds have a net warming effect on climate by reducing emission of LW radiation to space more effectively than they reflect SW radiation[100]. Cirrus clouds can form by two different mechanisms: homogeneous freezing, in which small solution droplets freeze spontaneously, and heterogeneous freezing, in which ice crystals form on INPs[91]. The latter mechanism requires only modest supersaturation but can only occur when sufficient INPs are present and typically results in low concentrations of large ice crystals. The former mechanism requires much higher supersaturation but does not rely on the presence of INPs and typically results in high concentrations of small ice crystals[12]. The transition from homogeneous to heterogeneous freezing has been estimated to occur for INP concentrations between 10 and 100 L^{-1}.[101]

The impact of dust on cirrus clouds is thus highly dependent on whether non-dust INPs are present (Fig. 2e). In conditions that favor heterogeneous freezing (high INP concentration), additional dust INPs would add ice crystals and reduce their size, while in conditions that favor homogeneous freezing (low INP concentration), additional dust could reduce the number of ice crystals and increase their size by shifting nucleation from occurring homogeneously to occurring heterogeneously. The former scenario would make cirrus clouds optically thicker and extend their lifetimes, while the latter scenario would do the opposite.

The perturbation of the TOA radiation budget would naturally be opposite in the two scenarios, and at present it is unclear which one dominates globally. Thus, although global modelling results of dust impacts on cirrus clouds have in the past produced net radiative perturbations of opposite sign[12], this difference does not signify a complete lack of process understanding, but rather indicates different assessments of which cirrus formation mechanism dominates in the absence of dust.

Research that incorporated up-to-date laboratory results of ice nucleation on dust particles[92,102,103] generally find an optical thinning of cirrus clouds due to dust (Fig. 2e, top schematic). This thinning yields large opposing perturbations to both LW and SW radiation at the TOA, but the LW effect tends to dominate, producing a net negative (cooling) perturbation[21,104] . The corresponding overall radiative effect was estimated at -0.4 Wm^{-2} using global simulations with the CAM5 model[104], whereas simulations for a more moderate dust change (going from 10% to 100% of present emissions) with a modified version of the same model[21] found a range from -0.32 to +0.05 Wm^{-2}. We therefore assess the perturbation of the TOA radiation budget due to dust effects on cirrus clouds to -0.20 Wm^{-2}, with a 90% confidence interval of -0.40 to +0.10 Wm^{-2}. This range encompasses the strongest reported cooling effects[104] as a lower bound and the possibility of a slight warming as an upper bound. We assign low confidence to this assessment due to the limited body of research.

Dust semi-direct effects on clouds

Absorption of radiation by mineral dust can modify the temperature profile[105], which can change atmospheric stability, the moisture profile, and secondary circulations, all of which can alter cloud distributions[106-108]. These processes, known as aerosol semi-direct effects (SDEs)[109,110], were broadly described in the IPCC's Sixth Assessment Report as atmospheric adjustments to instantaneous aerosol direct radiative effects without considering effects due to changes in surface temperature[25,28]. Because dust accounts for about a third of shortwave absorption by all aerosols, the contribution of dust to SDEe is crucial to accurately quantifying the overall dust effective radiative forcing[111,112].

The magnitude of the dust SDE, and whether it results in a positive (warming) or a negative (cooling) radiative effect, depends primarily on two factors: the relative position of the dust and cloud layers within the atmospheric column and the amount of radiation absorbed by the dust layer[106,107]. In turn, radiation absorption by dust depends on dust loading and microphysical properties, including dust mineralogical composition, shape, and size distribution[42,43,45,113].

Understanding of the pathways through which dust semi-directly impacts different cloud regimes follows that of SDEs produced by other absorbing aerosols, like black carbon[106,114]. For low-altitude clouds, the pathways for dust SDEs can be categorized into cases where the dust layer is above, within or near, and below the cloud layer (Fig. 2f). When dust is located above boundary-layer clouds, local heating by the above-cloud dust can stabilize the boundary layer by strengthening its capping inversion, causing an increased build-up of moisture in the boundary layer. This increased moisture increases the cloud cover, which results in a negative SDE (left schematic of Fig. 2f)[107,115]. Conversely, when dust is located within or near boundary-layer clouds, the local heating could result in reduction of relative humidity, which could evaporate the cloud and result in a positive SDE (middle schematic of Fig. 2f)[107,116]. Finally, when dust is located below boundary-layer clouds, the local heating may enhance convergence and available

moisture, increasing cloud cover and resulting in a negative SDE (right schematic of Fig. 2f)[117,118].

Radiation absorption by dust can also generate SDEs for mid and high-altitude clouds. These SDEs involve the compensation between the warming effect produced by dust absorption, which tends to decrease cloud cover, and an increase in moisture convergence, which tends to increase cloud cover[106]. Although the effect of the enhanced moisture convergence can overwhelm the warming effect, resulting in increased globally averaged high-altitude cloud cover during the summer, the overall annual-mean dust SDE is to decrease the high cloud cover[106,119,120].

This understanding of dust SDEs assumes that dust, like other absorbing aerosols such as black carbon, warms the atmospheric layer in which they are present[121]. This assumption is based on evidence that dust radiative warming due to SW absorption dominates over dust radiative cooling due to LW emission[122,123]. However, past research likely underestimated the amount of coarse dust, which emits LW radiation more strongly than fine dust[49,56]. Because accounting for the observed abundance coarse dust particles could produce substantial LW radiative cooling of the atmosphere[32,36,124], the understanding of the different pathways through which dust can semi-directly impact clouds remains incomplete.

Because of the uncertainties in the various pathways by which dust absorption semi-directly influences cloud cover (Fig. 2f), a global observational estimate of dust SDE is not currently available. Instead, observationally based assessments have focused on dust-dominated regions[107,116,125]. For example, satellite observations show that annual dust SDE is negative (-1.2 ± 1.4 Wm^{-2}) over the North Atlantic Ocean[107]. Since estimates of dust SDE show strong spatial variability and because dust SDE is driven by different dominant mechanisms for different cloud regimes over the ocean than over land[106], scaling such observationally based regional dust SDE estimates to global values is difficult. In addition, accurate retrievals of dust microphysical properties, including dust optical properties and size distribution, are lacking from global-scale satellite and ground-based platforms[112], making it difficult to obtain global estimates of dust SDE.

In the absence of global observational estimates, climate models simulations have reported a net positive global annual mean dust SDE[126]. These estimates vary by over an order of magnitude, between 0.01 and 0.16 Wm^{-2}, and depend on the climate model used[21,126,127]. These positive SDE estimates are consistent with an overall decrease in cloud cover in these simulations. Although model estimates of dust SDE and cloud changes are thus relatively consistent with each other, they could be biased because of unaccounted for uncertainties in dust absorption properties, the vertical distributions of dust and clouds, an underestimate of LW radiative cooling by coarse dust, and the parameterization of cloud processes[56,58,111]. Therefore, based on the above model simulations, the dust SDE is estimated at 0.07 ± 0.07 Wm^{-2}, but with low confidence due to these possible biases and limited research.

Interactions with the cryosphere

Dust interactions with the cryosphere impact climate by altering cryospheric conditions via dust direct and indirect radiative effects (Figs. 2a-f) and by darkening snow and ice surfaces after deposition (Fig. 2g), which leads to a positive surface radiative effect (Fig. 2g). This dust-induced snow albedo effect accelerates snow and glacier melting[18,128,129], which triggers a strong, positive surface albedo feedback on the climate system[130]. The dust-induced snow albedo effect is influenced by many factors, including dust concentration in snow[131,132], dust optical properties

as determined by its size distribution and chemical composition[132,133], dust-snow mixing state[134,135], snow grain size and shape[134], snowpack properties[136,137], and illumination conditions[132,138].

Observations indicate strong heterogeneity in dust concentrations in snow/ice. Along with different snowpack and atmospheric conditions, this variability in dust concentrations leads to large variations in the dust-induced snow albedo reduction and the associated surface radiative effects. For instance, the springtime dust-induced snow albedo effect is estimated to be less than 0.5 Wm^{-2} for the Arctic[139,140], up to 5 Wm^{-2} for remote mid-latitude snowpacks (such as the Tibetan Plateau)[139,141], and about 10–50 Wm^{-2} over polluted mid-latitude snowpacks (such as the U. S. Rocky Mountains)[18,128]. In some extremely polluted mid-latitude mountains, the local instantaneous snow albedo effect can be as high as 100–300 Wm^{-2} [142,143]. The dust-induced snow albedo effect is typically larger in aged snow than in fresh snow[18], because of the stronger light penetration and hence larger light absorption by dust in aged snow. Most research has focused on a few cryospheric hotspots in the Northern Hemisphere (the Rocky Mountains, Tibetan Plateau, European Alps, and the Arctic) during spring, when the dust-induced snow albedo effect is more prominent and often reaches its annual maximum.

There are only limited estimates of the global annual mean dust-induced snow albedo effect, with a central estimate of +0.013 Wm^{-2} and a 90% confidence interval of 0.007–0.03 Wm^{-2} [19,131,144]. Although the snow albedo radiative effect is smaller than most other dust radiative effects, it can still be more substantial regionally, particularly over polluted mid-latitude snowpacks[18].

Estimates of the dust-induced snow albedo effect are still associated with large uncertainties due to complicated and poorly constrained dust-snowpack-radiation interactions. Variations in the poorly constrained dust-snow mixing state, snow grain shape, dust size distribution and dust chemical composition can cause up to a factor of two uncertainty in the dust-induced snow albedo effect[134,135]. Moreover, the limited knowledge of dust evolution within the snowpack - for instance due to dust scavenging by melting water and dust enrichment at the snowpack surface - also adds to the uncertainty of the estimated snow albedo effect. Owing to the potential nonlinearity in dust-snow-radiation interactions and dust wet deposition, the dust-induced snow albedo effect may not increase linearly with dust concentration in the atmosphere or snowpack. Considering these uncertainties and the limited research, we assign low confidence to our estimate of the dust-induced snow albedo effect.

Interactions with biogeochemistry

Dust can influence ocean and land biogeochemistry, both directly through the addition of nutrients and pollutants to ecosystems, as well as indirectly through modifying precipitation, temperature, and radiation[20]. Atmospheric deposition of dust onto oceans provides iron, a limiting nutrient in high nutrient low chlorophyll (HNLC) regions[145,146]. In addition, nitrogen fixing organisms in the ocean have higher iron requirements, thereby linking iron deposition to the oceanic nitrogen cycle[147,148]. Although initial research suggested that atmospheric deposition was the dominant source of new iron[145,149], other ocean sources also have a substantial role in the iron cycle[150-152]. Overall, atmospheric inputs of iron to the ocean modulate ecosystem productivity and carbon sequestration on the timescale of decades[146,153].

, The soluble fraction of the iron is the most important for dust particles sinking through the ocean mixed layer. The deposition of soluble iron has increased since pre-industrial times, both

because of the historical increase of dust over this time period and because of an increase in iron solubilization during transport due to increased anthropogenic pollution[22,154,155]. Additionally, some other important sources of soluble iron have also increased, including from wildfires and anthropogenic combustion[156,157]. The resulting alleviation of iron limitation has increased ecosystem productivity, which in turn has reduced the atmospheric concentration of carbon dioxide and its radiative forcing (Fig. 2h).

Several ocean biogeochemical models include iron and its coupling to the nitrogen cycle and can therefore estimate the reduction of CO_2 concentrations due to the alleviation of iron limitation[158,159]. These models suggest that the increased deposition of soluble iron over the 20th century resulted in the uptake of ~4 ppm of CO_2, producing a radiative perturbation of -0.07 ± 0.07 Wm^{-2} [20,160]. Because approximately half of this increase in soluble iron was estimated to be due to a simulated ~40% increase in dust over the 20th century, these results imply a radiative effect due to dust-biogeochemistry interactions of -0.12 ± 0.12 Wm^{-2} (Eq. 1). Confidence in this assessment is very low, as it is based on only one study. Note that the radiative effect due to dust-biogeochemistry interactions differ from that due to other interactions in that its effect increases over time. Consequently, the radiative perturbation that it produces depends on the timescale.

Dust also contains phosphorus, a limiting nutrient in some tropical forests and grasslands[161,162], as well as in some ocean ecosystems[146,163]. For example, phosphorus from long-range transported North African dust may help maintain the productivity of the Amazon rainforest[164]. However, because inputs from atmospheric deposition of desert dust are thought to be important in the Amazon on millennial time scales[165] any contribution of changes in this phosphorus input probably produces a negligible contribution to dust radiative forcing since pre-industrial times. Dust also serves as a ballast, enhancing the downward transfer of organic material within the ocean, but there is not yet a quantitative estimate of the impacts in terms of productivity or carbon uptake feedback from this process[170,171]. In addition, desert dust could include elements that can be toxic to ocean or land ecosystems, such as Cu, although current estimates suggest that this effect is not important to Earth's radiation budget[172].

The dust effective radiative effect

To determine the climatic impact of past and future changes in atmospheric dust, it is critical to assess the dust effective radiative effect R (Eq. 2), which equals the sum of the various radiative effects generated by dust (Fig. 3). Many of these radiative effects oppose one another, resulting in a median estimate of R = -0.2 Wm^{-2}, with a wide 90% confidence interval of -0.7 to +0.3 Wm^{-2}. (Note that we neglected some rapid adjustments in assessing R, such as responses by water vapor and the lapse rate to dust direct radiative effects, but these adjustments are likely small[173].) As such, the net effect of dust on Earth's global radiation budget could be negligible, a substantial net cooling, or a small net warming.

On regional scales and for different seasons, the dust effective radiative effect can differ substantially from its global and annual mean in Figure 3. This regional and seasonal variability occurs because the various radiative effects are sensitive to the spatiotemporal variability in dust concentration, microphysical properties (mineralogy and size distribution), and environmental conditions (surface albedo and cloud cover). For instance, dust over reflective deserts likely produces substantial warming because of the high dust concentration, coarse size distribution[124], and because reflective surfaces reduce cooling produced by SW scattering and enhance warming

produced by SW absorption[35,174]. Similarly, dust likely produces net warming over snow and ice-covered regions because the high surface albedo enhances warming produced by dust absorption of SW radiation and because dust deposition decreases the surface albedo[42,131]. In contrast, dust over oceans usually produces cooling because dust is finer further from source regions and because the ocean albedo is only ~0.1 in the visible spectrum[175]. To determine the climate impacts of dust, it is thus critical not only to constrain the global mean dust effective radiative effect but also to constrain its spatiotemporal pattern.

Dust radiative forcing

Because dust produces a potentially large effective radiative effect, a change in atmospheric dust loading since pre-industrial times could have produced a substantial effective radiative forcing. Dust loading could have changed due to both climate change and widespread human land use changes (Box 1). Knowledge of the change in dust loading from pre-industrial to modern times depends largely on dust deposition records that resolve both the modern and the pre-industrial climate. Many of these deposition records show increases in dust deposition between modern and pre-industrial times, sometimes by a factor of ~4[23,169,176,177].

Dust reconstruction

We reconstructed the evolution of the global dust mass loading since pre-industrial times by combining 19 dust deposition records[23,169,176,177] with constraints on the source regions providing the deposition flux to each deposition core[8,44] (see Supplementary Information). This dust reconstruction used a bootstrap resampling method to propagate uncertainties in both the experimental deposition records and the constraints on source region-resolved deposition fluxes to each deposition site; nonetheless, errors should be interpreted as a lower bound.

The atmospheric loading of dust with a volume-equivalent diameter less than 20 μm has increased from 19 ± 6 Tg in the pre-industrial period (defined here as 1841-1860) to 29 ± 8 Tg in the modern climate (1981-2000). As such, global dust mass loading has increased by 55 ± 30 % (Fig. 4a). Although substantial, this increase is less than the doubling of dust suggested by previous research[22,23]. A large contributor to this increase has been Asian dust, which has increased by 74 ± 37 % from 8 ± 3 Tg in pre-industrial times to 13 ± 5 Tg in modern times (Fig. 4c). North African dust has increased less, from 10 ± 4 Tg in the pre-industrial period to 14 ± 4 Tg in the modern climate, representing a 46 (2-102) % increase. Both African and Asian dust mass loading peaked in the 1980s and then decreased substantially, consistent with changes observed from long-term dust concentration measurements, visibility records, and satellite observations[178-184]. Dust has likely also increased in the Southern Hemisphere, from 1.2 (0.6-2.2) Tg to 1.6 (0.8-2.2) Tg, representing a 27 (-14 to 88) % increase (Fig. 4d). Satellite observations suggest that global dust mass loading has been relatively stable since the year 2000, the end point of the analysis, with some notable regional trends, such as in Central and East Asia[185].

This large historical increase in dust mass loading is inadequately accounted for in current climate models and climate assessments. In fact, twelve climate models with prognostic dust cycles in the Coupled Model Intercomparison Project phase 6 (CMIP6) model ensemble[186,187] show little change in dust mass loading since pre-industrial times (Fig. 5). This failure of models to reproduce the historical dust increase could be due to several reasons (Box 1). If the dust increase has been largely driven by natural and anthropogenic climate changes, then the model failure could be either due to an inaccurate representation of these changes in models or because

modelled dust emissions are not sufficiently sensitive to changes in climate. This latter possibility is suggested by the common use in climate models of empirical dust source functions to parameterize the spatial distribution of dust emissions[188,189]. Because dust source functions are static, they mask physical links between changeable surface properties and dust emissions. As such, their use can cause models to underestimate the sensitivity of dust emissions to changes in climate[190]. Conversely, if the dust increase has been largely driven by human land use changes (Box 1), as suggested by research indicating that approximately a quarter of current dust emissions originate from regions heavily impacted by human land use[191] (Box 1), then the model failure to reproduce the dust increase could be caused by an underestimation of land use and land cover changes in drylands and the resulting increases in dust emissions.

Radiative forcing due to dust increase

The historical increase in dust loading could have produced a substantial radiative forcing. Combining R = -0.2 ± 0.5 Wm^{-2} with the 55 ± 30% historical dust loading increase yields a dust effective radiative forcing from 1841 to 2000 of $\Delta F_{p\rightarrow m}$ = -0.07 ± 0.18 Wm^{-2} . Dust radiative forcing could thus either have substantially contributed to, or slightly opposed, the total aerosol effective radiative forcing of -1.1 (-1.7 to -0.4) Wm^{-2} for the period of 1750 to 2019[28].

Note that the calculations of R and $\Delta F_{p\rightarrow m}$ are subject to important limitations. First, these calculations assume that radiative effects increase linearly with aerosol loading[6,192] (Eqs. 3 and 4). However, the increase of radiative effects with aerosol loading is usually less-than-linear, especially for interactions with clouds and biogeochemistry[20,21,26]. Moreover, the radiative effects of dust vary in space, such that $\Delta F_{p\rightarrow m}$ depends on the spatial pattern of dust increases, which the simple calculation here does not account for. For instance, Asian dust likely has an outsize impact on Northern Hemisphere cirrus clouds[98] and high latitude dust emissions are likely important in controlling the glaciation of mixed-phase clouds[193,194] but are not explicitly included in the dust reconstruction. Careful simulations with coupled climate models that reproduce the historical dust increase are thus needed to better constrain dust radiative forcing.

Because current climate models do not reproduce the historical dust increase, these models omit the potentially important radiative forcing due to increased dust interactions with radiation, clouds, atmospheric chemistry and the cryosphere. (Note that changes in CO_2 and other greenhouse gases due to dust interactions with biogeochemistry are inherently included in climate model runs forced by observed greenhouse gas concentrations.) Dust radiative forcing was thus not accounted for in constraints on the total aerosol effective radiative forcing in the IPCC Sixth Assessment Report[28]. Because constraints on climate sensitivity depend strongly on the aerosol radiative forcing since pre-industrial times[195], the failure by models and climate assessments to account for the historical increase in dust could thus have biased constraints on climate sensitivity and projections of future climate changes[196].

Future changes in dust radiative forcing

Future changes in dust radiative forcing are likely to be dominated by changes in atmospheric dust loading, which in turn will be determined by several factors. One important factor will be future changes in soil moisture since drier soils are more susceptible to aeolian erosion because of reduced soil cohesive forces and less vegetation[1,2]. In CMIP5 and CMIP6 models, changes in precipitation are the main driver of soil moisture changes, yet there is a wide degree of

divergence in model projections of precipitation[197]. Models do consistently show that as the planet warms the evaporative demand over land increases[198], which by itself would reduce soil moisture. However, the effects of reduced soil moisture may be countered by CO_2 fertilization, which reduces plant water losses. This could reduce dust emissions by driving an expansion of vegetation into arid regions[199], although the magnitude of this effect is uncertain[200]. Terrestrial stilling, the observed downward trend in surface wind speeds over land surfaces[201], could also affect dust emissions, with models suggesting a future reduction in Northern Hemisphere winds [202]. However, changes in atmospheric circulation patterns thought to impact surface wind speeds over dust producing regions may be more important[180]. Another consequence of planetary warming is an increase in precipitation variability[203], and thus extreme rainfall events[204], potentially increasing future sediment supply–and aeolian erosion–via alluvial and fluvial recharge[205]. Finally, future climate and land use changes could drive a decline in biological soil crusts that reduce dust emissions, which is a mechanism for increasing emissions that is not accounted for in current models[206].

Model estimates of future changes in dust are sensitive to methodology[207] and span the range of an increase in dust due to increasing aridity[208] to a decrease due to CO_2 fertilization driving an expansion of vegetation into arid regions[199,209]. Starting with CMIP5, simulations from some models included either prescribed dust emissions or fully interactive dust. However, both regional[189,210-212] and global[213] analyses of these models found that the dust mean state had substantial biases, that CMIP5 models did not reproduce historical dust variability, and that modelled dust emissions were insufficiently sensitive to changes in surface conditions. An analysis of dust changes over land in RCP 8.5 simulations, for which CO_2 emissions continue unabated throughout the 21st century, showed no secular trends in global dust[213]. An analysis of CMIP6 simulations demonstrated that many of these previously identified model deficiencies also exist in these newer climate model simulations (Fig. 5) and that the inter-model differences in dust are also growing relative to earlier CMIP efforts, suggesting that as model complexity increases so does model divergence in future projections of dust[214].

Given the inability of models to reproduce historical dust changes and the large spread in model projections of future dust change, it is not surprising that estimates of the change in dust radiative forcing per degree planetary warming, the so-called dust-climate feedback (units $Wm^{-2}K^{-1}$), is similarly uncertain. An analysis of the output from 6 CMIP6 models that participated in an aerosol intercomparison project found that these models differed in the sign of the dust-climate feedback[187], with a multimodel mean feedback of 0.0026 ± 0.0048 $Wm^{-2}K^{-1}$. Other research has speculated that a key driver of the model inconsistencies was the simulation of surface winds[187], which in turn may be related to the relatively coarse resolution of a typical climate model[215]. These results from CMIP6 are consistent with earlier research that estimated a multimodel mean feedback for CMIP5 models that was not statistically different from zero[216]. However, using a dust emission scheme that responded more realistically to changes in climate[217] enhanced the dust climate feedback due to changes in the dust direct radiative effect by an order of magnitude, yielding a range of -0.04 to +0.02 $Wm^{-2}K^{-1}$. On a regional scale, the dust climate feedback close to source regions is likely an additional order of magnitude larger[216].

Given the lack of confidence in model projections of future changes in the dust burden, and the substantial uncertainties in dust direct and indirect radiative effects, there is a low degree of confidence in the ability of models to predict future changes in the dust radiative forcing.

Summary & Future Perspectives

We assessed the global mean effective radiative effect of dust in the modern climate at R = -0.2 ± 0.5 Wm^{-2} (Fig. 3). Despite the considerable uncertainty in the sign and magnitude of R, which arises from the numerous uncertain and sometimes opposing mechanisms through which dust impacts climate, it is more likely that dust cools than that it warms global climate. We further found that global dust loading in the modern climate is 55 ± 30% higher than it was in pre-industrial times (Fig. 4), which has exerted a global mean effective radiative forcing of $\Delta F_{\mathrm{p\rightarrow m}} =$ -0.07 ± 0.18 Wm^{-2}. The historical increase in dust has thus likely somewhat counteracted greenhouse warming.

Current climate models fail to capture the historical increase in dust loading (Fig. 5) and thus inadequately account for dust radiative forcing, which could have caused biases in assessments of climate sensitivity and projections of future climate changes[195,196]. Substantial additional research is thus needed both to better constrain R and $\Delta F_{\mathrm{p\rightarrow m}}$ and to enable climate models to reproduce the historical increase in dust.

The dust direct radiative effect (DRE) contributes most to the uncertainty in R and $\Delta F_{\mathrm{p\rightarrow m}}$ (Fig. 3). Future research should focus on reducing its uncertainty by better constraining dust optical properties through *in situ* and remote sensing observations. For instance, the information on soil mineralogy to be provided by NASA's 2022 Earth Surface Mineral Dust Source Investigation (EMIT) mission could help constrain dust optical properties[218]. Additionally, models likely greatly underestimate the atmospheric concentration of super coarse dust[49,55,56,124], which warms by absorbing SW and LW radiation. This should be addressed by obtaining more measurements of emitted and transported dust that extend to the difficult-to-measure super coarse dust size range[29,36,54,55], and by developing improved parameterizations of super coarse dust emission[220] and deposition and implementing those in climate models.

Another priority for future research should be better constraining the radiative effects of dust due to interactions with clouds, anthropogenic aerosols, and biogeochemistry, which together contribute the remaining uncertainty in R (Fig. 3). Because of a dearth of observational constraints, our assessment of these radiative effects was mostly based on modelling studies. However, models struggle to correctly account for interactions of dust with clouds and anthropogenic aerosols, in part because of the mismatch in scales between the small scales at which the relevant processes occur and the large scales of climate model grid boxes[38,219,221]. As such, there is an urgent need for comprehensive *in situ* and satellite observations to constrain these interactions[12,193]. For instance, more satellite and in situ observations of cirrus interactions with dust and other INPs[98,99] could elucidate the relative importance of homogeneous and heterogeneous nucleation of ice crystals, which determines the sign of the radiative effect of dust interactions with cirrus (Fig. 2e)[12]. Furthermore, dust radiative effects due to interactions with clouds could be better constrained with future model simulations at a sufficiently high (kilometre-scale[221]) resolution to resolve the critical sub-grid scale turbulence and cloud processes that currently must be parameterized in models[219]. Finally, constraining radiative effects due to dust interactions with biogeochemistry requires an improved characterization of dust composition and how this evolves during transport, as well as accurate knowledge of which land and ocean regions are nutrient limited[153].

We also recommend that the community conducts multi-model experiments to obtain more robust estimates of the various dust radiative effects and of R and $\Delta F_{\mathrm{p\rightarrow m}}$. These experiments

should also investigate the uncertainty in radiative effects that result from model differences in dust optical properties, size distribution, model resolution, meteorology, the spatiotemporal distribution of dust emission fluxes, and parameterizations for dust deposition and dust interactions with clouds, radiation, atmospheric chemistry, the cryosphere, biogeochemistry, and other aerosols. Such multi-model experiments could be done in the context of the Aerosol Model Intercomparison project (AeroCom), which has previously performed multi-model experiments for anthropogenic aerosols[25,222].

Future research should also prioritize addressing the failure of models to reproduce the historical increase in dust (Fig. 5). Doing so requires an improved understanding of the factors driving changes in the atmospheric dust loading since pre-industrial times, including the relative roles of changes in land use, wind speed, soil properties, sediment supply, and vegetation cover[180,223]. Additionally, new observations and modelling are needed to clarify the meteorological processes that generate the high wind speeds that produce dust, such as cold pool outflows from moist convection[215,224,225], and to improve the representation of those processes in climate models. Finally, more physically based dust emission schemes need to be developed and implemented into climate models. These schemes should explicitly account for dust emissions from high latitudes, which have an outsize effect on climate through interactions with clouds[193,194]. Furthermore, dust emission schemes should avoid using empirical dust source functions as these do not respond to changes in climate; instead, emission schemes should use process understanding to account for the dependence of the spatiotemporal pattern and mineralogical composition of dust emissions on wind, soil properties, sediment supply, and vegetation coverage[190,226,227]. A challenge will be to achieve this without making these schemes too sensitive to parameters such as soil moisture that non-linearly increase dust emissions[1,2] and that have considerable variability in climate models[197]. These fundamental improvements in dust emission schemes are also needed for meaningful predictions of future changes in dust and for more accurate predictions of dust impacts on regional climate.

References

1 Shao, Y. P. *Physics and Modelling of Wind Erosion*. 2nd edn, (Springer, 2008).

2 Kok, J. F., Parteli, E. J. R., Michaels, T. I. & Karam, D. B. The physics of wind-blown sand and dust. *Rep. Prog. Phys.* **75**, 106901, doi:10.1088/0034-4885/75/10/106901 (2012).

3 Gillette, D. A. On the production of soil wind erosion having the potential for long range transport. *J. Rech. Atmos.* **8**, 734-744 (1974).

4 Kok, J. F. A scaling theory for the size distribution of emitted dust aerosols suggests climate models underestimate the size of the global dust cycle. *Proc. Natl. Acad. Sci. U. S. A.* **108**, 1016-1021, doi:10.1073/pnas.1014798108 (2011).

5 Mahowald, N. *et al.* The size distribution of desert dust aerosols and its impact on the Earth system. *Aeolian Res.* **15**, 53-71, doi:10.1016/j.aeolia.2013.09.002 (2014).

6 Kok, J. F. *et al.* Smaller desert dust cooling effect estimated from analysis of dust size and abundance. *Nature Geoscience* **10**, 274-278, doi:10.1038/ngeo2912 (2017).

7 Gliss, J. *et al.* AeroCom phase III multi-model evaluation of the aerosol life cycle and optical properties using ground- and space-based remote sensing as well as surface in situ observations. *Atmospheric Chemistry and Physics* **21**, 87-128, doi:10.5194/acp-21-87-2021 (2021).

8 Kok, J. F. *et al.* Contribution of the world's main dust source regions to the global cycle of desert dust. *Atmospheric Chemistry and Physics* **21**, 8169-8193, doi:10.5194/acp-21-8169-2021 (2021).
9 Bullard, J. E. *et al.* High-latitude dust in the Earth system. *Reviews of Geophysics* **54**, 447-485, doi:10.1002/2016rg000518 (2016).
10 Prospero, J. M., Delany, A. C. & Carlson, T. N. The Discovery of African Dust Transport to the Western Hemisphere and the Saharan Air Layer. *Bulletin of the American Meteorological Society* **102**, E1239-E1260, doi:10.1175/bams-d-19-0309.1 (2021).
11 Highwood, E. J. & Ryder, C. L. in *Mineral Dust: A Key Player in the Earth System* (eds Peter Knippertz & Jan-Berend W. Stuut) 327-357 (Springer Netherlands, 2014).
12 Storelvmo, T. Aerosol Effects on Climate via Mixed-Phase and Ice Clouds. *Annual Review of Earth and Planetary Sciences, Vol 45* **45**, 199-222, doi:10.1146/annurev-earth-060115-012240 (2017).
13 Karydis, V. A. *et al.* Global impact of mineral dust on cloud droplet number concentration. *Atmospheric Chemistry and Physics* **17**, 5601-5621, doi:10.5194/acp-17-5601-2017 (2017).
14 Klingmuller, K., Karydis, V. A., Bacer, S., Stenchikov, G. L. & Lelieveld, J. Weaker cooling by aerosols due to dust-pollution interactions. *Atmospheric Chemistry and Physics* **20**, 15285-15295, doi:10.5194/acp-20-15285-2020 (2020).
15 Klingmuller, K., Lelieveld, J., Karydis, V. A. & Stenchikov, G. L. Direct radiative effect of dust-pollution interactions. *Atmospheric Chemistry and Physics* **19**, 7397-7408, doi:10.5194/acp-19-7397-2019 (2019).
16 Bauer, S. E. *et al.* Do sulfate and nitrate coatings on mineral dust have important effects on radiative properties and climate modeling? *J. Geophys. Res.-Atmos.* **112**, doi:10.1029/2005jd006977 (2007).
17 Usher, C. R., Michel, A. E. & Grassian, V. H. Reactions on mineral dust. *Chemical Reviews* **103**, 4883-4939, doi:10.1021/cr020657y (2003).
18 Skiles, S. M., Flanner, M., Cook, J. M., Dumont, M. & Painter, T. H. Radiative forcing by light-absorbing particles in snow. *Nature Climate Change* **8**, 965-+, doi:10.1038/s41558-018-0296-5 (2018).
19 Tuccella, P., Pitari, G., Colaiuda, V., Raparelli, E. & Curci, G. Present-day radiative effect from radiation-absorbing aerosols in snow. *Atmospheric Chemistry and Physics* **21**, 6875-6893, doi:10.5194/acp-21-6875-2021 (2021).
20 Mahowald, N. Aerosol Indirect Effect on Biogeochemical Cycles and Climate. *Science* **334**, 794-796, doi:10.1126/science.1207374 (2011).
21 McGraw, Z., Storelvmo, T., David, R. O. & Sagoo, N. Global Radiative Impacts of Mineral Dust Perturbations Through Stratiform Clouds. *Journal of Geophysical Research-Atmospheres* **125**, doi:10.1029/2019jd031807 (2020).
22 Mahowald, N. M. *et al.* Observed 20th century desert dust variability: impact on climate and biogeochemistry. *Atmos. Chem. Phys.* **10**, 10875-10893, doi:10.5194/acp-10-10875-2010 (2010).
23 Hooper, J. & Marx, S. A global doubling of dust emissions during the Anthropocene? *Glob. Planet. Change* **169**, 70-91, doi:10.1016/j.gloplacha.2018.07.003 (2018).
24 Boucher, O. & Tanre, D. Estimation of the aerosol perturbation to the Earth's radiative budget over oceans using POLDER satellite aerosol retrievals. *Geophysical Research Letters* **27**, 1103-1106, doi:10.1029/1999gl010963 (2000).

25 Boucher, O. *et al.* in *Climate Change 2013: The Physical Science Basis. Contribution of Working Group I to the Fifth Assessment Report of the Intergovernmental Panel on Climate Change* (eds T.F. Stocker *et al.*) pp. 571–658 (Cambridge University Press, 2013).
26 Carslaw, K. S. *et al.* Large contribution of natural aerosols to uncertainty in indirect forcing. *Nature* **503**, 67-+, doi:10.1038/nature12674 (2013).
27 Forster, P. *et al.* in *Climate Change 2007: The Physical Science Basis.* (ed S. Solomon, D. Qin, M. Manning, Z. Chen, M. Marquis, K.B. Averyt, M.Tignor and H.L. Miller) (Cambridge University Press, 2007).
28 Forster, P. *et al.* (eds V. Masson-Delmotte *et al.*) Ch. Chapter 7: The Earth's energy budget, climate feedbacks, and climate sensitivity, (2021).
29 Ryder, C. L. *et al.* Optical properties of Saharan dust aerosol and contribution from the coarse mode as measured during the Fennec 2011 aircraft campaign. *Atmospheric Chemistry and Physics* **13**, 303-325, doi:10.5194/acp-13-303-2013 (2013).
30 Tegen, I. & Lacis, A. A. Modeling of particle size distribution and its influence on the radiative properties of mineral dust aerosol. *Journal of Geophysical Research-Atmospheres* **101**, 19237-19244 (1996).
31 Sokolik, I. N. & Toon, O. B. Incorporation of mineralogical composition into models of the radiative properties of mineral aerosol from UV to IR wavelengths. *Journal of Geophysical Research-Atmospheres* **104**, 9423-9444, doi:10.1029/1998jd200048 (1999).
32 Di Biagio, C., Balkanski, Y., Albani, S., Boucher, O. & Formenti, P. Direct Radiative Effect by Mineral Dust Aerosols Constrained by New Microphysical and Spectral Optical Data. *Geophysical Research Letters* **47**, doi:10.1029/2019gl086186 (2020).
33 Dufresne, J. L., Gautier, C., Ricchiazzi, P. & Fouquart, Y. Longwave scattering effects of mineral aerosols. *J. Atmos. Sci.* **59**, 1959-1966, doi:10.1175/1520-0469(2002)059<1959:lseoma>2.0.co;2 (2002).
34 Bohren, C. F. & Huffman, D. R. *Absorption and Scattering of Light by Small Particles*. (Wiley, 1983).
35 Liou, K. N. *An Introduction to Atmospheric Radiation*. Second edn, (Academic Press, 2002).
36 Adebiyi, A. A. *et al.* A review of coarse mineral dust in the Earth system. *EarthArXiv preprint*, doi:10.31223/X5QD36 (2022).
37 Di Biagio, C. *et al.* Complex refractive indices and single-scattering albedo of global dust aerosols in the shortwave spectrum and relationship to size and iron content. *Atmospheric Chemistry and Physics* **19**, 15503-15531, doi:10.5194/acp-19-15503-2019 (2019).
38 Riemer, N., Ault, A. P., West, M., Craig, R. L. & Curtis, J. H. Aerosol Mixing State: Measurements, Modeling, and Impacts. *Reviews of Geophysics* **57**, 187-249, doi:10.1029/2018rg000615 (2019).
39 Renard, J. B. *et al.* In situ measurements of desert dust particles above the western Mediterranean Sea with the balloon-borne Light Optical Aerosol Counter/sizer (LOAC) during the ChArMEx campaign of summer 2013. *Atmospheric Chemistry and Physics* **18**, 3677-3699, doi:10.5194/acp-18-3677-2018 (2018).
40 Denjean, C. *et al.* Size distribution and optical properties of African mineral dust after intercontinental transport. *Journal of Geophysical Research-Atmospheres* **121**, 7117-7138, doi:10.1002/2016jd024783 (2016).

41 Seinfeld, J. H. *et al.* ACE-ASIA - Regional climatic and atmospheric chemical effects of Asian dust and pollution. *Bull. Am. Meteorol. Soc.* **85**, 367-380, doi:10.1175/bams-85-3-367 (2004).
42 Liao, H. & Seinfeld, J. H. Radiative forcing by mineral dust aerosols: sensitivity to key variables. *Journal of Geophysical Research-Atmospheres* **103**, 31637-31645 (1998).
43 Claquin, T., Schulz, M., Balkanski, Y. & Boucher, O. Uncertainties in assessing radiative forcing by mineral dust. *Tellus Ser. B-Chem. Phys. Meteorol.* **50**, 491-505, doi:10.1034/j.1600-0889.1998.t01-2-00007.x (1998).
44 Kok, J. F. *et al.* Improved representation of the global dust cycle using observational constraints on dust properties and abundance. *Atmospheric Chemistry and Physics* **21**, 8127-8167, doi:10.5194/acp-21-8127-2021 (2021).
45 Di Biagio, C. *et al.* Global scale variability of the mineral dust long-wave refractive index: a new dataset of in situ measurements for climate modeling and remote sensing. *Atmospheric Chemistry and Physics* **17**, 1901-1929, doi:10.5194/acp-17-1901-2017 (2017).
46 Li, L. L. *et al.* Quantifying the range of the dust direct radiative effect due to source mineralogy uncertainty. *Atmospheric Chemistry and Physics* **21**, 3973-4005, doi:10.5194/acp-21-3973-2021 (2021).
47 Sicard, M., Bertolin, S., Mallet, M., Dubuisson, P. & Comeron, A. Estimation of mineral dust long-wave radiative forcing: sensitivity study to particle properties and application to real cases in the region of Barcelona. *Atmospheric Chemistry and Physics* **14**, 9213-9231, doi:10.5194/acp-14-9213-2014 (2014).
48 Brindley, H. E. & Russell, J. E. An assessment of Saharan dust loading and the corresponding cloud-free longwave direct radiative effect from geostationary satellite observations. *Journal of Geophysical Research-Atmospheres* **114**, doi:10.1029/2008jd011635 (2009).
49 Adebiyi, A. A. & Kok, J. F. Climate models miss most of the coarse dust in the atmosphere. *Science Advances* **6**, eaaz9507, doi:10.1126/sciadv.aaz9507 (2020).
50 Tuccella, P., Curci, G., Pitari, G., Lee, S. & Jo, D. S. Direct Radiative Effect of Absorbing Aerosols: Sensitivity to Mixing State, Brown Carbon, and Soil Dust Refractive Index and Shape. *Journal of Geophysical Research-Atmospheres* **125**, doi:10.1029/2019jd030967 (2020).
51 Albani, S. *et al.* Improved dust representation in the Community Atmosphere Model. *J. Adv. Model. Earth Sy.* **6**, 541-570, doi:10.1002/2013ms000279 (2014).
52 Ito, A., Adebiyi, A. A., Huang, Y. & Kok, J. F. Less atmospheric radiative heating by dust due to the synergy of coarser size and aspherical shape. *Atmospheric Chemistry and Physics* **21**, 16869-16891, doi:10.5194/acp-21-16869-2021 (2021).
53 Colarco, P. R. *et al.* Impact of radiatively interactive dust aerosols in the NASA GEOS-5 climate model: Sensitivity to dust particle shape and refractive index. *Journal of Geophysical Research-Atmospheres* **119**, 753-786, doi:10.1002/2013jd020046 (2014).
54 Ryder, C. L. *et al.* Coarse-mode mineral dust size distributions, composition and optical properties from AER-D aircraft measurements over the tropical eastern Atlantic. *Atmospheric Chemistry and Physics* **18**, 17225-17257, doi:10.5194/acp-18-17225-2018 (2018).

55 Weinzierl, B. *et al.* The Saharan Aerosol Long-range Transport and Aerosol-Cloud Interaction Experiment (SALTRACE): overview and selected highlights. *Bull. Am. Meteorol. Soc.* **98**, 1427-1451, doi:10.1175/BAMS-D-15-00142.1 (2017).
56 Ansmann, A. *et al.* Profiling of Saharan dust from the Caribbean to West Africa, Part 2: Shipborne lidar measurements versus forecasts. *Atmospheric Chemistry and Physics Discussions*, doi:10.5194/acp-2017-502 (2017).
57 Song, Q. *et al.* Toward an Observation-Based Estimate of Dust Net Radiative Effects in Tropical North Atlantic Through Integrating Satellite Observations and In Situ Measurements of Dust Properties. *Atmos. Chem. Phys. Discuss.* **in review** (2018).
58 O'Sullivan, D. *et al.* Models transport Saharan dust too low in the atmosphere: a comparison of the MetUM and CAMS forecasts with observations. *Atmospheric Chemistry and Physics* **20**, 12955-12982, doi:10.5194/acp-20-12955-2020 (2020).
59 Kim, D. *et al.* Sources, sinks, and transatlantic transport of North African dust aerosol: A multimodel analysis and comparison with remote sensing data. *Journal of Geophysical Research-Atmospheres* **119**, 6259-6277, doi:10.1002/2013jd021099 (2014).
60 Karydis, V. A., Tsimpidi, A. P., Lei, W., Molina, L. T. & Pandis, S. N. Formation of semivolatile inorganic aerosols in the Mexico City Metropolitan Area during the MILAGRO campaign. *Atmospheric Chemistry and Physics* **11**, 13305-13323, doi:10.5194/acp-11-13305-2011 (2011).
61 Formenti, P., Elbert, W., Maenhaut, W., Haywood, J. & Andreae, M. O. Chemical composition of mineral dust aerosol during the Saharan Dust Experiment (SHADE) airborne campaign in the Cape Verde region, September 2000. *Journal of Geophysical Research-Atmospheres* **108**, doi:10.1029/2002jd002648 (2003).
62 Begue, N. *et al.* Aerosol processing and CCN formation of an intense Saharan dust plume during the EUCAARI 2008 campaign. *Atmospheric Chemistry and Physics* **15**, 3497-3516, doi:10.5194/acp-15-3497-2015 (2015).
63 Li, W. J. & Shao, L. Y. Observation of nitrate coatings on atmospheric mineral dust particles. *Atmospheric Chemistry and Physics* **9**, 1863-1871, doi:10.5194/acp-9-1863-2009 (2009).
64 Karydis, V. A., Tsimpidi, A. P., Pozzer, A., Astitha, M. & Lelieveld, J. Effects of mineral dust on global atmospheric nitrate concentrations. *Atmospheric Chemistry and Physics* **16**, 1491-1509, doi:10.5194/acp-16-1491-2016 (2016).
65 Sullivan, R. C., Guazzotti, S. A., Sodeman, D. A. & Prather, K. A. Direct observations of the atmospheric processing of Asian mineral dust. *Atmospheric Chemistry and Physics* **7**, 1213-1236 (2007).
66 Huang, X. *et al.* Pathways of sulfate enhancement by natural and anthropogenic mineral aerosols in China. *Journal of Geophysical Research-Atmospheres* **119**, 14165-14179, doi:10.1002/2014jd022301 (2014).
67 Sullivan, R. C. *et al.* Mineral dust is a sink for chlorine in the marine boundary layer. *Atmos. Environ.* **41**, 7166-7179, doi:10.1016/j.atmosenv.2007.05.047 (2007).
68 Feng, T. *et al.* Summertime ozone formation in Xi'an and surrounding areas, China. *Atmospheric Chemistry and Physics* **16**, 4323-4342, doi:10.5194/acp-16-4323-2016 (2016).
69 Gharibzadeh, M., Bidokhti, A. A. & Alam, K. The interaction of ozone and aerosol in a semi-arid region in the Middle East: Ozone formation and radiative forcing implications. *Atmos. Environ.* **245**, doi:10.1016/j.atmosenv.2020.118015 (2021).

70 Usher, C. R., Al-Hosney, H., Carlos-Cuellar, S. & Grassian, V. H. A laboratory study of the heterogeneous uptake and oxidation of sulfur dioxide on mineral dust particles. *Journal of Geophysical Research-Atmospheres* **107**, doi:10.1029/2002jd002051 (2002).
71 Goodman, A. L., Underwood, G. M. & Grassian, V. H. Heterogeneous reaction of NO2: Characterization of gas-phase and adsorbed products from the reaction, 2NO(2)(g)+H2O(a)-> HONO(g)+HNO3(a) on hydrated silica particles. *Journal of Physical Chemistry A* **103**, 7217-7223, doi:10.1021/jp9910688 (1999).
72 Nenes, A., Pandis, S. N., Weber, R. J. & Russell, A. Aerosol pH and liquid water content determine when particulate matter is sensitive to ammonia and nitrate availability. *Atmospheric Chemistry and Physics* **20**, 3249-3258, doi:10.5194/acp-20-3249-2020 (2020).
73 Karydis, V. A., Tsimpidi, A. P., Pozzer, A. & Lelieveld, J. How alkaline compounds control atmospheric aerosol particle acidity. *Atmospheric Chemistry and Physics* **21**, 14983-15001, doi:10.5194/acp-21-14983-2021 (2021).
74 Trochkine, D. *et al.* Mineral aerosol particles collected in Dunhuang, China, and their comparison with chemically modified particles collected over Japan. *Journal of Geophysical Research-Atmospheres* **108**, doi:10.1029/2002jd003268 (2003).
75 Fitzgerald, E., Ault, A. P., Zauscher, M. D., Mayol-Bracero, O. L. & Prather, K. A. Comparison of the mixing state of long-range transported Asian and African mineral dust. *Atmos. Environ.* **115**, 19-25, doi:10.1016/j.atmosenv.2015.04.031 (2015).
76 Klingmuller, K. *et al.* Revised mineral dust emissions in the atmospheric chemistry-climate model EMAC (MESSy 2.52 DU_Astitha1 KKDU2017 patch). *Geoscientific Model Development* **11**, 989-1008, doi:10.5194/gmd-11-989-2018 (2018).
77 Perlwitz, J. P., Perez Garcia-Pando, C. & Miller, R. L. Predicting the mineral composition of dust aerosols - Part 1: Representing key processes. *Atmos. Chem. Phys.* **15**, 11593-11627 (2015).
78 Sullivan, R. C. *et al.* Effect of chemical mixing state on the hygroscopicity and cloud nucleation properties of calcium mineral dust particles. *Atmospheric Chemistry and Physics* **9**, 3303-3316, doi:10.5194/acp-9-3303-2009 (2009).
79 Tang, M. J., Cziczo, D. J. & Grassian, V. H. Interactions of Water with Mineral Dust Aerosol: Water Adsorption, Hygroscopicity, Cloud Condensation, and Ice Nucleation. *Chemical Reviews* **116**, 4205-4259, doi:10.1021/acs.chemrev.5b00529 (2016).
80 Cziczo, D. J. *et al.* Deactivation of ice nuclei due to atmospherically relevant surface coatings. *Environmental Research Letters* **4**, doi:10.1088/1748-9326/4/4/044013 (2009).
81 Fan, S. M., Horowitz, L. W., Levy, H. & Moxim, W. J. Impact of air pollution on wet deposition of mineral dust aerosols. *Geophysical Research Letters* **31**, doi:10.1029/2003gl018501 (2004).
82 Liao, H., Seinfeld, J. H., Adams, P. J. & Mickley, L. J. Global radiative forcing of coupled tropospheric ozone and aerosols in a unified general circulation model. *Journal of Geophysical Research-Atmospheres* **109**, D16207, doi:10.1029/2003jd004456 (2004).
83 Bauer, S. E. & Koch, D. Impact of heterogeneous sulfate formation at mineral dust surfaces on aerosol loads and radiative forcing in the Goddard Institute for Space Studies general circulation model. *Journal of Geophysical Research-Atmospheres* **110**, doi:10.1029/2005jd005870 (2005).
84 Koehler, K. A. *et al.* Hygroscopicity and cloud droplet activation of mineral dust aerosol. *Geophysical Research Letters* **36**, doi:10.1029/2009gl037348 (2009).

85 Kumar, P., Sokolik, I. N. & Nenes, A. Measurements of cloud condensation nuclei activity and droplet activation kinetics of fresh unprocessed regional dust samples and minerals. *Atmospheric Chemistry and Physics* **11**, 3527-3541, doi:10.5194/acp-11-3527-2011 (2011).
86 Gaston, C. J. Re-examining Dust Chemical Aging and Its Impacts on Earth's Climate. *Accounts of Chemical Research* **53**, 1005-1013, doi:10.1021/acs.accounts.0c00102 (2020).
87 Karydis, V. A., Kumar, P., Barahona, D., Sokolik, I. N. & Nenes, A. On the effect of dust particles on global cloud condensation nuclei and cloud droplet number. *Journal of Geophysical Research-Atmospheres* **116**, doi:10.1029/2011jd016283 (2011).
88 Sagoo, N. & Storelvmo, T. Testing the sensitivity of past climates to the indirect effects of dust. *Geophysical Research Letters* **44**, 5807-5817, doi:10.1002/2017gl072584 (2017).
89 Li, R., Min, Q. L. & Harrison, L. C. A Case Study: The Indirect Aerosol Effects of Mineral Dust on Warm Clouds. *J. Atmos. Sci.* **67**, 805-816, doi:10.1175/2009jas3235.1 (2010).
90 Hoose, C. & Mohler, O. Heterogeneous ice nucleation on atmospheric aerosols: a review of results from laboratory experiments. *Atmospheric Chemistry and Physics* **12**, 9817-9854, doi:10.5194/acp-12-9817-2012 (2012).
91 Kanji, Z. A. *et al.* Overview of Ice Nucleating Particles. *Ice Formation and Evolution in Clouds and Precipitation: Measurement and Modeling Challenges* **58**, doi:10.1175/amsmonographs-d-16-0006.1 (2017).
92 David, R. O. *et al.* Pore condensation and freezing is responsible for ice formation below water saturation for porous particles. *Proc. Natl. Acad. Sci. U. S. A.* **116**, 8184-8189, doi:10.1073/pnas.1813647116 (2019).
93 Matus, A. V. & L'Ecuyer, T. S. The role of cloud phase in Earth's radiation budget. *Journal of Geophysical Research-Atmospheres* **122**, 2559-2578, doi:10.1002/2016jd025951 (2017).
94 Morrison, H. *et al.* Resilience of persistent Arctic mixed-phase clouds. *Nature Geoscience* **5**, 11-17, doi:10.1038/ngeo1332 (2012).
95 Shi, Y. & Liu, X. H. Dust Radiative Effects on Climate by Glaciating Mixed-Phase Clouds. *Geophysical Research Letters* **46**, 6128-6137, doi:10.1029/2019gl082504 (2019).
96 Choi, Y. S., Lindzen, R. S., Ho, C. H. & Kim, J. Space observations of cold-cloud phase change. *Proc. Natl. Acad. Sci. U. S. A.* **107**, 11211-11216, doi:10.1073/pnas.1006241107 (2010).
97 Tan, I., Storelvmo, T. & Choi, Y. S. Spaceborne lidar observations of the ice-nucleating potential of dust, polluted dust, and smoke aerosols in mixed-phase clouds. *Journal of Geophysical Research-Atmospheres* **119**, 6653-6665, doi:10.1002/2013jd021333 (2014).
98 Froyd, K. D. *et al.* Dominant role of mineral dust in cirrus cloud formation revealed by global-scale measurements. *Nature Geoscience* **15**, 177-+, doi:10.1038/s41561-022-00901-w (2022).
99 Cziczo, D. J. *et al.* Clarifying the Dominant Sources and Mechanisms of Cirrus Cloud Formation. *Science* **340**, 1320-1324, doi:10.1126/science.1234145 (2013).
100 Heymsfield, A. J. *et al.* Cirrus Clouds. *Ice Formation and Evolution in Clouds and Precipitation: Measurement and Modeling Challenges* **58**, doi:10.1175/amsmonographs-d-16-0010.1 (2017).

101 Storelvmo, T. & Herger, N. Cirrus cloud susceptibility to the injection of ice nuclei in the upper troposphere. *Journal of Geophysical Research-Atmospheres* **119**, 2375-2389, doi:10.1002/2013jd020816 (2014).
102 DeMott, P. J. *et al.* Integrating laboratory and field data to quantify the immersion freezing ice nucleation activity of mineral dust particles. *Atmospheric Chemistry and Physics* **15**, 393-409, doi:10.5194/acp-15-393-2015 (2015).
103 Ullrich, R. *et al.* A New Ice Nucleation Active Site Parameterization for Desert Dust and Soot. *J. Atmos. Sci.* **74**, 699-717, doi:10.1175/jas-d-16-0074.1 (2017).
104 Liu, X. *et al.* Sensitivity studies of dust ice nuclei effect on cirrus clouds with the Community Atmosphere Model CAM5. *Atmospheric Chemistry and Physics* **12**, 12061-12079, doi:10.5194/acp-12-12061-2012 (2012).
105 Huang, J. P., Wang, T. H., Wang, W. C., Li, Z. Q. & Yan, H. R. Climate effects of dust aerosols over East Asian arid and semiarid regions. *Journal of Geophysical Research-Atmospheres* **119**, 11398-11416, doi:10.1002/2014jd021796 (2014).
106 Perlwitz, J. & Miller, R. L. Cloud cover increase with increasing aerosol absorptivity: A counterexample to the conventional semidirect aerosol effect. *Journal of Geophysical Research-Atmospheres* **115**, doi:10.1029/2009jd012637 (2010).
107 Amiri-Farahani, A., Allen, R. J., Neubauer, D. & Lohmann, U. Impact of Saharan dust on North Atlantic marine stratocumulus clouds: importance of the semidirect effect. *Atmospheric Chemistry and Physics* **17**, 6305-6322, doi:10.5194/acp-17-6305-2017 (2017).
108 DeFlorio, M. J. *et al.* Semidirect dynamical and radiative effect of North African dust transport on lower tropospheric clouds over the subtropical North Atlantic in CESM 1.0. *Journal of Geophysical Research-Atmospheres* **119**, doi:10.1002/2013jd020997 (2014).
109 Hansen, J., Sato, M. & Ruedy, R. Radiative forcing and climate response. *Journal of Geophysical Research-Atmospheres* **102**, 6831-6864, doi:10.1029/96jd03436 (1997).
110 Ackerman, A. S. *et al.* Reduction of tropical cloudiness by soot. *Science* **288**, 1042-1047, doi:10.1126/science.288.5468.1042 (2000).
111 Sand, M. *et al.* Aerosol absorption in global models from AeroCom phase III. *Atmospheric Chemistry and Physics* **21**, 15929-15947, doi:10.5194/acp-21-15929-2021 (2021).
112 Samset, B. H. *et al.* Aerosol Absorption: Progress Towards Global and Regional Constraints. *Current Climate Change Reports* **4**, 65-83 (2018).
113 Russell, P. B. *et al.* Absorption Angstrom Exponent in AERONET and related data as an indicator of aerosol composition. *Atmospheric Chemistry and Physics* **10**, 1155-1169, doi:10.5194/acp-10-1155-2010 (2010).
114 Koch, D. & Del Genio, A. D. Black carbon semi-direct effects on cloud cover: review and synthesis. *Atmospheric Chemistry and Physics* **10**, 7685-7696, doi:10.5194/acp-10-7685-2010 (2010).
115 Doherty, O. M. & Evan, A. T. Identification of a new dust-stratocumulus indirect effect over the tropical North Atlantic. *Geophysical Research Letters* **41**, 6935-6942, doi:10.1002/2014gl060897 (2014).
116 Huang, J. P. *et al.* Satellite-based assessment of possible dust aerosols semi-direct effect on cloud water path over East Asia. *Geophysical Research Letters* **33**, doi:10.1029/2006gl026561 (2006).

117 McFarquhar, G. M. & Wang, H. L. Effects of aerosols on trade wind cumuli over the Indian Ocean: Model simulations. *Quarterly Journal of the Royal Meteorological Society* **132**, 821-843, doi:10.1256/qj.04.179 (2006).
118 Feingold, G., Jiang, H. L. & Harrington, J. Y. On smoke suppression of clouds in Amazonia. *Geophysical Research Letters* **32**, doi:10.1029/2004gl021369 (2005).
119 Stephens, G. L., Wood, N. B. & Pakula, L. A. On the radiative effects of dust on tropical convection. *Geophysical Research Letters* **31**, doi:10.1029/2004gl021342 (2004).
120 Miller, R. L., Tegen, I. & Perlwitz, J. Surface radiative forcing by soil dust aerosols and the hydrologic cycle. *Journal of Geophysical Research-Atmospheres* **109**, D04203, doi:10.1029/2003jd004085 (2004).
121 Wong, S., Dessler, A. E., Mahowald, N. M., Yang, P. & Feng, Q. Maintenance of Lower Tropospheric Temperature Inversion in the Saharan Air Layer by Dust and Dry Anomaly. *Journal of Climate* **22**, 5149-5162, doi:10.1175/2009jcli2847.1 (2009).
122 Zhu, A., Ramanathan, V., Li, F. & Kim, D. Dust plumes over the Pacific, Indian, and Atlantic oceans: Climatology and radiative impact. *Journal of Geophysical Research-Atmospheres* **112**, doi:10.1029/2007jd008427 (2007).
123 Chen, S. H., Wang, S. H. & Waylonis, M. Modification of Saharan air layer and environmental shear over the eastern Atlantic Ocean by dust-radiation effects. *Journal of Geophysical Research-Atmospheres* **115**, D21202, doi:D2120210.1029/2010jd014158 (2010).
124 Ryder, C. L. *et al.* Coarse and giant particles are ubiquitous in Saharan dust export regions and are radiatively significant over the Sahara. *Atmospheric Chemistry and Physics* **19**, 15353-15376, doi:10.5194/acp-19-15353-2019 (2019).
125 Huang, J. P. *et al.* Possible influences of Asian dust aerosols on cloud properties and radiative forcing observed from MODIS and CERES. *Geophysical Research Letters* **33**, doi:10.1029/2005gl024724 (2006).
126 Amiri-Farahani, A., Allen, R. J., Li, K. F. & Chu, J. E. The Semidirect Effect of Combined Dust and Sea Salt Aerosols in a Multimodel Analysis. *Geophysical Research Letters* **46**, 10512-10521, doi:10.1029/2019gl084590 (2019).
127 Tegen, I. & Heinold, B. Large-Scale Modeling of Absorbing Aerosols and Their Semi-Direct Effects. *Atmosphere* **9**, doi:10.3390/atmos9100380 (2018).
128 Painter, T. H. *et al.* Response of Colorado River runoff to dust radiative forcing in snow. *Proc. Natl. Acad. Sci. U. S. A.* **107**, 17125-17130, doi:10.1073/pnas.0913139107 (2010).
129 Lee, W. L. *et al.* Impact of absorbing aerosol deposition on snow albedo reduction over the southern Tibetan plateau based on satellite observations. *Theoretical and Applied Climatology* **129**, 1373-1382, doi:10.1007/s00704-016-1860-4 (2017).
130 Hall, A. The role of surface albedo feedback in climate. *Journal of Climate* **17**, 1550-1568, doi:10.1175/1520-0442(2004)017<1550:trosaf>2.0.co;2 (2004).
131 Flanner, M. G. *et al.* Springtime warming and reduced snow cover from carbonaceous particles. *Atmospheric Chemistry and Physics* **9**, 2481-2497 (2009).
132 Dang, C., Brandt, R. E. & Warren, S. G. Parameterizations for narrowband and broadband albedo of pure snow and snow containing mineral dust and black carbon. *Journal of Geophysical Research-Atmospheres* **120**, 5446-5468, doi:10.1002/2014jd022646 (2015).

133 Flanner, M. G. *et al.* SNICAR-ADv3: a community tool for modeling spectral snow albedo. *Geoscientific Model Development* **14**, 7673-7704, doi:10.5194/gmd-14-7673-2021 (2021).
134 Liou, K. N. *et al.* Stochastic parameterization for light absorption by internally mixed BC/dust in snow grains for application to climate models. *Journal of Geophysical Research-Atmospheres* **119**, 7616-7632, doi:10.1002/2014jd021665 (2014).
135 He, C. L., Liou, K. N., Takano, Y., Chen, F. & Barlage, M. Enhanced Snow Absorption and Albedo Reduction by Dust-Snow Internal Mixing: Modeling and Parameterization. *J. Adv. Model. Earth Syst.* **11**, 3755-3776, doi:10.1029/2019ms001737 (2019).
136 Warren, S. G. & Wiscombe, W. J. A Model For The Spectral Albedo Of Snow .2. Snow Containing Atmospheric Aerosols. *J. Atmos. Sci.* **37**, 2734-2745, doi:10.1175/1520-0469(1980)037<2734:amftsa>2.0.co;2 (1980).
137 He, C., Takano, Y. & Liou, K. N. Close packing effects on clean and dirty snow albedo and associated climatic implications. *Geophysical Research Letters* **44**, 3719-3727, doi:10.1002/2017gl072916 (2017).
138 He, C. & Flanner, M. Snow Albedo and Radiative Transfer: Theory, Modeling, and Parameterization. *Springer Series in Light Scattering, Vol 5: Radiative Transfer, Remote Sensing, and Light Scattering*, 67-133, doi:10.1007/978-3-030-38696-2_3 (2020).
139 Dang, C. *et al.* Measurements of light-absorbing particles in snow across the Arctic, North America, and China: Effects on surface albedo. *Journal of Geophysical Research-Atmospheres* **122**, 10149-10168, doi:10.1002/2017jd027070 (2017).
140 Kylling, A., Zwaaftink, C. D. G. & Stohl, A. Mineral Dust Instantaneous Radiative Forcing in the Arctic. *Geophysical Research Letters* **45**, 4290-4298, doi:10.1029/2018gl077346 (2018).
141 Dong, Z. W. *et al.* Aeolian dust transport, cycle and influences in high-elevation cryosphere of the Tibetan Plateau region: New evidences from alpine snow and ice. *Earth-Sci. Rev.* **211**, doi:10.1016/j.earscirev.2020.103408 (2020).
142 Di Mauro, B. *et al.* Mineral dust impact on snow radiative properties in the European Alps combining ground, UAV, and satellite observations. *Journal of Geophysical Research-Atmospheres* **120**, 6080-6097, doi:10.1002/2015jd023287 (2015).
143 Skiles, S. M. & Painter, T. H. Toward Understanding Direct Absorption and Grain Size Feedbacks by Dust Radiative Forcing in Snow With Coupled Snow Physical and Radiative Transfer Modeling. *Water Resour. Res.* **55**, 7362-7378, doi:10.1029/2018wr024573 (2019).
144 Lawrence, D. M. *et al.* The CCSM4 Land Simulation, 1850-2005: Assessment of Surface Climate and New Capabilities. *Journal of Climate* **25**, 2240-2260, doi:10.1175/jcli-d-11-00103.1 (2012).
145 Martin, J. H. Glacial-interglacial CO2 change: The iron hypothesis. *Paleoceanography* **5**, 1-13, doi:10.1029/PA005i001p00001 (1990).
146 Moore, C. M. *et al.* Processes and patterns of oceanic nutrient limitation. *Nature Geoscience* **6**, 701-710, doi:10.1038/ngeo1765 (2013).
147 Capone, D. G., Zehr, J. P., Paerl, H. W., Bergman, B. & Carpenter, E. J. Trichodesmium, a globally significant marine cyanobacterium. *Science* **276**, 1221-1229, doi:10.1126/science.276.5316.1221 (1997).
148 Moore, J. K., Doney, S. C., Lindsay, K., Mahowald, N. & Michaels, A. F. Nitrogen fixation amplifies the ocean biogeochemical response to decadal timescale variations in

mineral dust deposition. *Tellus Ser. B-Chem. Phys. Meteorol.* **58**, 560-572, doi:10.1111/j.1600-0889.2006.00209.x (2006).
149 Fung, I. Y. *et al.* Iron supply and demand in the upper ocean. *Global Biogeochemical Cycles* **14**, 281-295, doi:10.1029/1999gb900059 (2000).
150 Lam, P. J. & Bishop, J. K. B. The continental margin is a key source of iron to the HNLC North Pacific Ocean. *Geophysical Research Letters* **35**, doi:10.1029/2008gl033294 (2008).
151 Moore, J. K. & Braucher, O. Sedimentary and mineral dust sources of dissolved iron to the world ocean. *Biogeosciences* **5**, 631-656, doi:10.5194/bg-5-631-2008 (2008).
152 Parekh, P., Follows, M. J. & Boyle, E. Modeling the global ocean iron cycle. *Global Biogeochemical Cycles* **18**, doi:10.1029/2003gb002061 (2004).
153 Mahowald, N. M. *et al.* Aerosol trace metal leaching and impacts on marine microorganisms. *Nature Communications* **9**, doi:10.1038/s41467-018-04970-7 (2018).
154 Johnson, M. S. & Meskhidze, N. Atmospheric dissolved iron deposition to the global oceans: effects of oxalate-promoted Fe dissolution, photochemical redox cycling, and dust mineralogy. *Geoscientific Model Development* **6**, 1137-1155, doi:10.5194/gmd-6-1137-2013 (2013).
155 Meskhidze, N., Chameides, W. L. & Nenes, A. Dust and pollution: A recipe for enhanced ocean fertilization? *Journal of Geophysical Research-Atmospheres* **110**, doi:10.1029/2004jd005082 (2005).
156 Chuang, P. Y., Duvall, R. M., Shafer, M. M. & Schauer, J. J. The origin of water soluble particulate iron in the Asian atmospheric outflow. *Geophysical Research Letters* **32**, doi:10.1029/2004gl021946 (2005).
157 Guieu, C., Bonnet, S., Wagener, T. & Loye-Pilot, M. D. Biomass burning as a source of dissolved iron to the open ocean? *Geophysical Research Letters* **32**, doi:10.1029/2005gl022962 (2005).
158 Tagliabue, A. *et al.* The integral role of iron in ocean biogeochemistry. *Nature* **543**, 51-59, doi:10.1038/nature21058 (2017).
159 Krishnamurthy, A., Moore, J. K., Mahowald, N., Luo, C. & Zender, C. S. Impacts of atmospheric nutrient inputs on marine biogeochemistry. *Journal of Geophysical Research-Biogeosciences* **115**, doi:10.1029/2009jg001115 (2010).
160 Mahowald, N. *et al.* Desert dust and anthropogenic aerosol interactions in the Community Climate System Model coupled-carbon-climate model. *Biogeosciences* **8**, 387-414, doi:10.5194/bg-8-387-2011 (2011).
161 Okin, G. S. *et al.* Spatial patterns of soil nutrients in two southern African savannas. *Journal of Geophysical Research-Biogeosciences* **113**, doi:10.1029/2007jg000584 (2008).
162 Vitousek, P. M. Litterfall, nutrient cycling, and nutrient limitation in tropical forests. *Ecology* **65**, 285-298, doi:10.2307/1939481 (1984).
163 Falkowski, P. G., Barber, R. T. & Smetacek, V. Biogeochemical controls and feedbacks on ocean primary production. *Science* **281**, 200-206, doi:10.1126/science.281.5374.200 (1998).
164 Swap, R., Garstang, M., Greco, S., Talbot, R. & Kallberg, P. Saharan dust in the amazon basin. *Tellus Ser. B-Chem. Phys. Meteorol.* **44**, 133-149, doi:10.1034/j.1600-0889.1992.t01-1-00005.x (1992).

165 Okin, G. S., Mahowald, N., Chadwick, O. A. & Artaxo, P. Impact of desert dust on the biogeochemistry of phosphorus in terrestrial ecosystems. *Global Biogeochemical Cycles* **18**, Gb2005, doi:10.1029/2003gb002145 (2004).
166 Barkley, A. E. *et al.* African biomass burning is a substantial source of phosphorus deposition to the Amazon, Tropical Atlantic Ocean, and Southern Ocean. *Proc. Natl. Acad. Sci. U. S. A.* **116**, 16216-16221, doi:10.1073/pnas.1906091116 (2019).
167 Mahowald, N. M. *et al.* Impacts of biomass burning emissions and land use change on Amazonian atmospheric phosphorus cycling and deposition. *Global Biogeochemical Cycles* **19**, doi:10.1029/2005gb002541 (2005).
168 Okin, G. S. *et al.* Impacts of atmospheric nutrient deposition on marine productivity: Roles of nitrogen, phosphorus, and iron. *Global Biogeochemical Cycles* **25**, doi:10.1029/2010gb003858 (2011).
169 McConnell, J. R., Aristarain, A. J., Banta, J. R., Edwards, P. R. & Simoes, J. C. 20th-Century doubling in dust archived in an Antarctic Peninsula ice core parallels climate change and desertification in South America. *Proc. Natl. Acad. Sci. U. S. A.* **104**, 5743-5748, doi:10.1073/pnas.0607657104 (2007).
170 Armstrong, R. A., Lee, C., Hedges, J. I., Honjo, S. & Wakeham, S. G. A new, mechanistic model for organic carbon fluxes in the ocean based on the quantitative association of POC with ballast minerals. *Deep-Sea Res. Part II-Top. Stud. Oceanogr.* **49**, 219-236, doi:10.1016/s0967-0645(01)00101-1 (2001).
171 van der Jagt, H., Friese, C., Stuut, J. B. W., Fischer, G. & Iversen, M. H. The ballasting effect of Saharan dust deposition on aggregate dynamics and carbon export: Aggregation, settling, and scavenging potential of marine snow. *Limnology and Oceanography* **63**, 1386-1394, doi:10.1002/lno.10779 (2018).
172 Paytan, A. *et al.* Toxicity of atmospheric aerosols on marine phytoplankton. *Proc. Natl. Acad. Sci. U. S. A.* **106**, 4601-4605, doi:10.1073/pnas.0811486106 (2009).
173 Thornhill, G. D. *et al.* Effective radiative forcing from emissions of reactive gases and aerosols - a multi-model comparison. *Atmospheric Chemistry and Physics* **21**, 853-874, doi:10.5194/acp-21-853-2021 (2021).
174 Patadia, F., Yang, E. S. & Christopher, S. A. Does dust change the clear sky top of atmosphere shortwave flux over high surface reflectance regions? *Geophysical Research Letters* **36**, L15825, doi:10.1029/2009gl039092 (2009).
175 Jin, Z. H., Charlock, T. P., Smith, W. L. & Rutledge, K. A parameterization of ocean surface albedo. *Geophysical Research Letters* **31**, doi:10.1029/2004gl021180 (2004).
176 Mulitza, S. *et al.* Increase in African dust flux at the onset of commercial agriculture in the Sahel region. *Nature* **466**, 226-228, doi:10.1038/nature09213 (2010).
177 Clifford, H. M. *et al.* A 2000 Year Saharan Dust Event Proxy Record from an Ice Core in the European Alps. *Journal of Geophysical Research-Atmospheres* **124**, 12882-12900, doi:10.1029/2019jd030725 (2019).
178 Prospero, J. M. & Lamb, P. J. African droughts and dust transport to the Caribbean: Climate change implications. *Science* **302**, 1024-1027 (2003).
179 Evan, A. T. & Mukhopadhyay, S. African Dust over the Northern Tropical Atlantic: 1955-2008. *Journal of Applied Meteorology and Climatology* **49**, 2213-2229, doi:10.1175/2010jamc2485.1 (2010).
180 Evan, A. T., Flamant, C., Gaetani, M. & Guichard, F. The past, present and future of African dust. *Nature* **531**, 493-495 (2016).

181 Mahowald, N. M., Ballantine, J. A., Feddema, J. & Ramankutty, N. Global trends in visibility: implications for dust sources. *Atmospheric Chemistry and Physics* **7**, 3309-3339 (2007).
182 Shao, Y. P., Klose, M. & Wyrwoll, K. H. Recent global dust trend and connections to climate forcing. *Journal of Geophysical Research-Atmospheres* **118**, 11107-11118, doi:10.1002/jgrd.50836 (2013).
183 Wang, X., Huang, J. P., Ji, M. X. & Higuchi, K. Variability of East Asia dust events and their long-term trend. *Atmos. Environ.* **42**, 3156-3165, doi:10.1016/j.atmosenv.2007.07.046 (2008).
184 Zuidema, P. *et al.* Is Summer African Dust Arriving Earlier to Barbados? The Updated Long-Term In Situ Dust Mass Concentration Time Series from Ragged Point, Barbados, and Miami, Florida. *Bulletin of the American Meteorological Society* **100**, 1981-1986, doi:10.1175/bams-d-18-0083.1 (2019).
185 Gkikas, A. *et al.* Quantification of the dust optical depth across spatiotemporal scales with the MIDAS global dataset (2003-2017). *Atmospheric Chemistry and Physics* **22**, 3553-3578, doi:10.5194/acp-22-3553-2022 (2022).
186 Eyring, V. *et al.* Overview of the Coupled Model Intercomparison Project Phase 6 (CMIP6) experimental design and organization. *Geoscientific Model Development* **9**, 1937-1958, doi:10.5194/gmd-9-1937-2016 (2016).
187 Thornhill, G. *et al.* Climate-driven chemistry and aerosol feedbacks in CMIP6 Earth system models. *Atmospheric Chemistry and Physics* **21**, 1105-1126, doi:10.5194/acp-21-1105-2021 (2021).
188 Ginoux, P. *et al.* Sources and distributions of dust aerosols simulated with the GOCART model. *J. Geophys. Res.* **106**, 20255-20273 (2001).
189 Wu, C. C., Lin, Z. & Liu, X. The global dust cycle and uncertainty in CMIP5 (Coupled Model Intercomparison Project phase 5) models. *Atmospheric Chemistry and Physics* **20**, 10401-10425, doi:10.5194/acp-20-10401-2020 (2020).
190 Kok, J. F., Albani, S., Mahowald, N. M. & Ward, D. S. An improved dust emission model - Part 2: Evaluation in the Community Earth System Model, with implications for the use of dust source functions. *Atmos. Chem. Phys.* **14**, 13043-13061, doi:10.5194/acp-14-13043-2014 (2014).
191 Ginoux, P., Prospero, J. M., Gill, T. E., Hsu, N. C. & Zhao, M. Global-scale attribution of anthropogenic and natural dust sources and their emission rates based on MODIS Deep Blue aerosol products. *Reviews of Geophysics* **50**, Rg3005, doi:10.1029/2012rg000388 (2012).
192 Stevens, B. Rethinking the Lower Bound on Aerosol Radiative Forcing. *J. Climate* **28**, 4794-4819, doi:10.1175/jcli-d-14-00656.1 (2015).
193 Murray, B. J., Carslaw, K. S. & Field, P. R. Opinion: Cloud-phase climate feedback and the importance of ice-nucleating particles. *Atmospheric Chemistry and Physics* **21**, 665-679, doi:10.5194/acp-21-665-2021 (2021).
194 Shi, Y. *et al.* Relative importance of high-latitude local and long-range-transported dust for Arctic ice-nucleating particles and impacts on Arctic mixed-phase clouds. *Atmospheric Chemistry and Physics* **22**, 2909-2935, doi:10.5194/acp-22-2909-2022 (2022).
195 Andreae, M. O., Jones, C. D. & Cox, P. M. Strong present-day aerosol cooling implies a hot future. *Nature* **435**, 1187-1190, doi:10.1038/nature03671 (2005).

196 Sherwood, S. C. *et al.* An Assessment of Earth's Climate Sensitivity Using Multiple Lines of Evidence. *Reviews of Geophysics* **58**, doi:10.1029/2019rg000678 (2020).
197 Caretta, M. A. *et al.* in *Climate Change 2022: Impacts, Adaptation, and Vulnerability. Contribution of Working Group II to the Sixth Assessment Report of the Intergovernmental Panel on Climate Change.* (eds H.-O. Pörtner *et al.*) (Cambridge University Press, 2022).
198 Cook, B. I. *et al.* Twenty-First Century Drought Projections in the CMIP6 Forcing Scenarios. *Earth Future* **8**, doi:10.1029/2019ef001461 (2020).
199 Mahowald, N. M. & Luo, C. A less dusty future? *Geophysical Research Letters* **30**, 1903, doi:10.1029/2003gl017880 (2003).
200 Smith, W. K. *et al.* Large divergence of satellite and Earth system model estimates of global terrestrial CO2 fertilization. *Nature Climate Change* **6**, 306-310, doi:10.1038/nclimate2879 (2016).
201 McVicar, T. R. *et al.* Global review and synthesis of trends in observed terrestrial near-surface wind speeds: Implications for evaporation. *J. Hydrol.* **416**, 182-205, doi:10.1016/j.jhydrol.2011.10.024 (2012).
202 Zha, J. L. *et al.* Projected changes in global terrestrial near-surface wind speed in 1.5 degrees C-4.0 degrees C global warming levels. *Environmental Research Letters* **16**, doi:10.1088/1748-9326/ac2fdd (2021).
203 Pendergrass, A. G., Knutti, R., Lehner, F., Deser, C. & Sanderson, B. M. Precipitation variability increases in a warmer climate. *Scientific Reports* **7**, doi:10.1038/s41598-017-17966-y (2017).
204 O'Gorman, P. A. & Schneider, T. The physical basis for increases in precipitation extremes in simulations of 21st-century climate change. *Proc. Natl. Acad. Sci. U. S. A.* **106**, 14773-14777, doi:10.1073/pnas.0907610106 (2009).
205 Zender, C. S. & Kwon, E. Y. Regional contrasts in dust emission responses to climate. *Journal of Geophysical Research-Atmospheres* **110**, doi:10.1029/2004jd005501 (2005).
206 Rodriguez-Caballero, E. *et al.* Global cycling and climate effects of aeolian dust controlled by biological soil crusts. *Nature Geoscience* **15**, 458-+, doi:10.1038/s41561-022-00942-1 (2022).
207 Tegen, I., Werner, M., Harrison, S. P. & Kohfeld, K. E. Relative importance of climate and land use in determining present and future global soil dust emission. *Geophysical Research Letters* **31**, doi:10.1029/2003gl019216 (2004).
208 Woodward, S., Roberts, D. L. & Betts, R. A. A simulation of the effect of climate change-induced desertification on mineral dust aerosol. *Geophysical Research Letters* **32**, L18810, doi:10.1029/2005gl023482 (2005).
209 Mahowald, N. M. *et al.* Change in atmospheric mineral aerosols in response to climate: Last glacial period, preindustrial, modern, and doubled carbon dioxide climates. *J. Geophys. Res.* **111**, D10202, doi:10.1029/2005jd006653 (2006).
210 Evan, A. T., Flamant, C., Fiedler, S. & Doherty, O. An analysis of aeolian dust in climate models. *Geophys. Res. Lett.* **41**, 5996-6001, doi:10.1002/2014GL060545 (2014).
211 Evan, A. T. Surface Winds and Dust Biases in Climate Models. *Geophysical Research Letters* **45**, 1079-1085, doi:10.1002/2017gl076353 (2018).
212 Wu, C. L. *et al.* Can Climate Models Reproduce the Decadal Change of Dust Aerosol in East Asia? *Geophysical Research Letters* **45**, 9953-9962, doi:10.1029/2018gl079376 (2018).

213 Pu, B. & Ginoux, P. How reliable are CMIP5 models in simulating dust optical depth? *Atmospheric Chemistry and Physics* **18**, 12491-12510, doi:10.5194/acp-18-12491-2018 (2018).
214 Zhao, A., Ryder, C. L. & Wilcox, L. J. How well do the CMIP6 models simulate dust aerosols? *Atmospheric Chemistry and Physics* **22**, 2095-2119, doi:10.5194/acp-22-2095-2022 (2022).
215 Heinold, B. *et al.* The role of deep convection and nocturnal low-level jets for dust emission in summertime West Africa: Estimates from convection-permitting simulations. *Journal of Geophysical Research-Atmospheres* **118**, 4385-4400, doi:10.1002/jgrd.50402 (2013).
216 Kok, J. F., Ward, D. S., Mahowald, N. M. & Evan, A. T. Global and regional importance of the direct dust-climate feedback. *Nature Communications* **9**, doi:10.1038/s41467-017-02620-y (2018).
217 Kok, J. F. *et al.* An improved dust emission model - Part 1: Model description and comparison against measurements. *Atmos. Chem. Phys.* **14**, 13023-13041, doi:10.5194/acp-14-13023-2014 (2014).
218 Green, R. O. *et al.* in *IEEE Aerospace Conference.* (2020).
219 National Academies of Sciences, E., and Medicine. *Reflecting Sunlight: Recommendations for Solar Geoengineering Research and Research Governance*. (The National Academies Press, 2021).
220 Meng, J. *et al.* Improved Parameterization for the Size Distribution of Emitted Dust Aerosols Reduces Model Underestimation of Super Coarse Dust. *Geophysical Research Letters* **49**, doi:10.1029/2021gl097287 (2022).
221 Slingo, J. *et al.* Ambitious partnership needed for reliable climate prediction. *Nature Climate Change* **12**, 499-503, doi:10.1038/s41558-022-01384-8 (2022).
222 Myhre, G. *et al.* Radiative forcing of the direct aerosol effect from AeroCom Phase II simulations. *Atmospheric Chemistry and Physics* **13**, 1853-1877, doi:10.5194/acp-13-1853-2013 (2013).
223 Okin, G. S. Where and How Often Does Rain Prevent Dust Emission? *Geophysical Research Letters* **49**, doi:10.1029/2021gl095501 (2022).
224 Bergametti, G. *et al.* Rain, Wind, and Dust Connections in the Sahel. *Journal of Geophysical Research-Atmospheres* **127**, doi:10.1029/2021jd035802 (2022).
225 Marsham, J. H., Knippertz, P., Dixon, N. S., Parker, D. J. & Lister, G. M. S. The importance of the representation of deep convection for modeled dust-generating winds over West Africa during summer. *Geophysical Research Letters* **38**, doi:10.1029/2011gl048368 (2011).
226 Okin, G. S. A new model of wind erosion in the presence of vegetation. *Journal of Geophysical Research-Earth Surface* **113**, F02s10, doi:10.1029/2007jf000758 (2008).
227 Chappell, A. & Webb, N. P. Using albedo to reform wind erosion modelling, mapping and monitoring. *Aeolian Research* **23**, 63-78, doi:10.1016/j.aeolia.2016.09.006 (2016).
228 Huang, J. P. *et al.* Global semi-arid climate change over last 60 years. *Clim. Dyn.* **46**, 1131-1150, doi:10.1007/s00382-015-2636-8 (2016).
229 Prospero, J. M., Ginoux, P., Torres, O., Nicholson, S. E. & Gill, T. E. Environmental characterization of global sources of atmospheric soil dust identified with the Nimbus 7 Total Ozone Mapping Spectrometer (TOMS) absorbing aerosol product. *Reviews of Geophysics* **40**, 1002, doi:10.1029/2000rg000095 (2002).

230 Stanelle, T., Bey, I., Raddatz, T., Reick, C. & Tegen, I. Anthropogenically induced changes in twentieth century mineral dust burden and the associated impact on radiative forcing. *Journal of Geophysical Research-Atmospheres* **119**, 13526-13546, doi:10.1002/2014jd022062 (2014).
231 Kohfeld, K. E. & Harrison, S. P. DIRTMAP: the geological record of dust. *Earth-Sci. Rev.* **54**, 81-114 (2001).
232 Markle, B. R., Steig, E. J., Roe, G. H., Winckler, G. & McConnell, J. R. Concomitant variability in high-latitude aerosols, water isotopes and the hydrologic cycle. *Nature Geoscience* **11**, 853-+, doi:10.1038/s41561-018-0210-9 (2018).
233 Cowie, S. M., Knippertz, P. & Marsham, J. H. Are vegetation-related roughness changes the cause of the recent decrease in dust emission from the Sahel? *Geophysical Research Letters* **40**, 1868-1872, doi:10.1002/grl.50273 (2013).
234 Smith, S. D. *et al.* Elevated CO2 increases productivity and invasive species success in an arid ecosystem. *Nature* **408**, 79-82 (2000).
235 Mahowald, N. M. Anthropocene changes in desert area: Sensitivity to climate model predictions. *Geophysical Research Letters* **34**, L18817, doi:10.1029/2007gl030472 (2007).
236 Goldewijk, K. K., Beusen, A., van Drecht, G. & de Vos, M. The HYDE 3.1 spatially explicit database of human-induced global land-use change over the past 12,000 years. *Global Ecology and Biogeography* **20**, 73-86, doi:10.1111/j.1466-8238.2010.00587.x (2011).
237 Lee, J. A., Baddock, M. C., Mbuh, M. J. & Gill, T. E. Geomorphic and land cover characteristics of aeolian dust sources in West Texas and eastern New Mexico, USA. *Aeolian Research* **3**, 459-466, doi:10.1016/j.aeolia.2011.08.001 (2012).
238 Neff, J. C. *et al.* Increasing eolian dust deposition in the western United States linked to human activity. *Nature Geoscience* **1**, 189-195, doi:10.1038/ngeo133 (2008).
239 Webb, N. P. & Pierre, C. Quantifying Anthropogenic Dust Emissions. *Earth Future* **6**, 286-295, doi:10.1002/2017ef000766 (2018).
240 Niemeyer, T. C. *et al.* Optical depth, size distribution and flux of dust from Owens Lake, California. *Earth Surface Processes and Landforms* **24**, 463-479, doi:10.1002/(sici)1096-9837(199905)24:5<463::aid-esp2>3.0.co;2-r (1999).
241 Xi, X. & Sokolik, I. N. Quantifying the anthropogenic dust emission from agricultural land use and desiccation of the Aral Sea in Central Asia. *Journal of Geophysical Research-Atmospheres* **121**, 12270-12281, doi:10.1002/2016jd025556 (2016).
242 Indoitu, R. *et al.* Dust emission and environmental changes in the dried bottom of the Aral Sea. *Aeolian Research* **17**, 101-115, doi:10.1016/j.aeolia.2015.02.004 (2015).
243 Tegen, I. & Fung, I. Contribution to the atmospheric mineral aerosol load from land-surface modification. *Journal of Geophysical Research-Atmospheres* **100**, 18707-18726, doi:10.1029/95jd02051 (1995).
244 Sokolik, I. N. & Toon, O. B. Direct radiative forcing by anthropogenic airborne mineral aerosols. *Nature* **381**, 681-683 (1996).
245 Mahowald, N. M., Rivera, G. D. R. & Luo, C. Comment on "Relative importance of climate and land use in determining present and future global soil dust emission" by I. Tegen et al. *Geophysical Research Letters* **31**, doi:10.1029/2004gl021272 (2004).

Acknowledgements

J.F.K. is funded by the National Science Foundation (NSF) grants 1552519 and 1856389, A.T.E. is funded by NSF grant 1833173, N.M.M. is funded by Department of Energy (DOE) grant DE-SC0021302, and V.A.K. is supported by the European Union via its Horizon 2020 project FORCeS (GA 81205). We thank James Hooper and Pierre Sabatier for providing dust deposition data.

Competing interests

The authors declare no competing interests.

Author contributions

J.F.K. led the review, performed the dust reconstruction, wrote the Supplementary material, prepared the figures, and compiled the paper. T.S. and A.A.A. contributed the section on clouds and figures 2c-f. V.A.K. contributed the section on atmospheric chemistry and figure 2b. N.M.M. contributed the section on biogeochemistry and a draft of figure 2h. C.H. contributed the section on the cryosphere and figure 2g. A.T.E. contributed the section on future dust changes. D.M.L. contributed to the CMIP6 results in figure 5. All authors contributed to the manuscript preparation, discussion and writing.

Supplementary information

Supplementary information is available for this paper at https://doi.org/10.1038/s415XX-XXX-XXXX-X

Data availability

The dust reconstruction data shown in Figure 4 are available at [link to be added upon article acceptance].

Figure legends

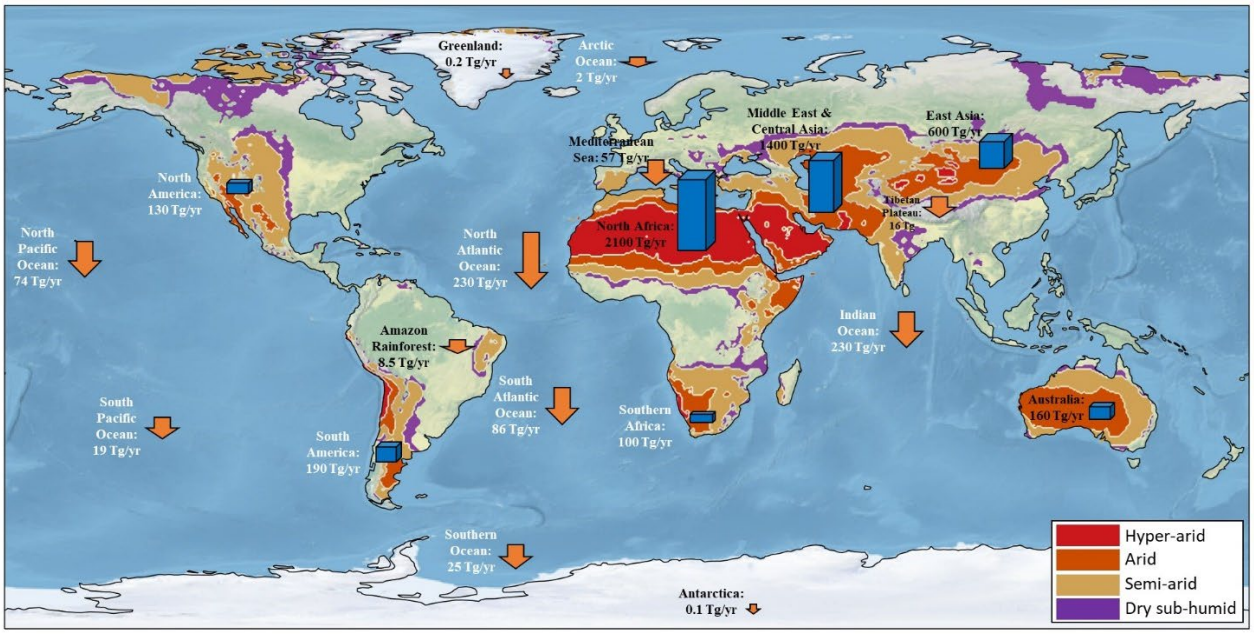

Figure 1. Main sources and sinks of dust in the global dust cycle. Emission fluxes (blue bars) from the world's main dust source regions and deposition fluxes (orange arrows) to regions where dust can impact surface albedo or biogeochemistry. Fluxes are for dust with geometric (volume-equivalent) diameter up to 20 μm and are based on constraints for 2004-2008[44]; emissions from high latitude regions are not included. Shading represents dryland classification based on the aridity index: hyper-arid regions (AI <

0.05; red shading), arid regions (0.05 < AI < 0.20; orange shading), semi-arid regions (0.20 < AI < 0.50; light brown shading), and dry sub-humid regions (0.50 < AI < 0.65; green shading)[228]. Most dust is emitted from drylands in North Africa and Asia, which are collectively known as the "dust belt"[229].

a Dust interactions with radiation

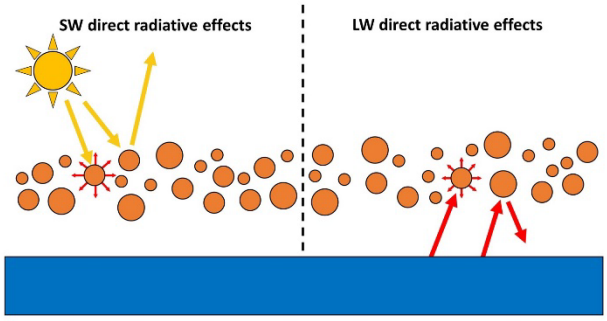

b Dust interactions with atmospheric chemistry

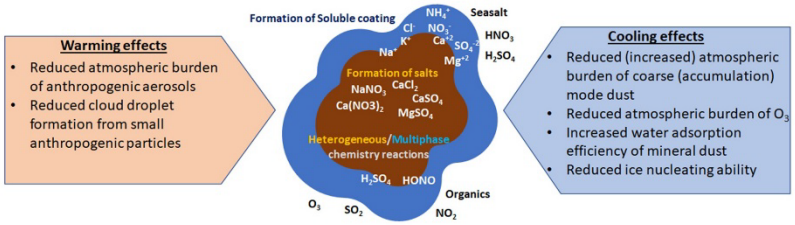

Dust interactions with clouds

c Dust indirect effects on warm clouds

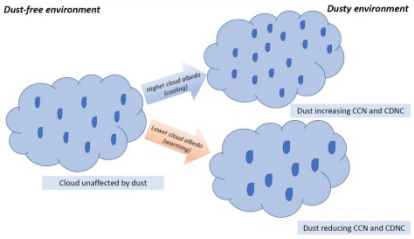

d Dust indirect effects on mixed-phase clouds

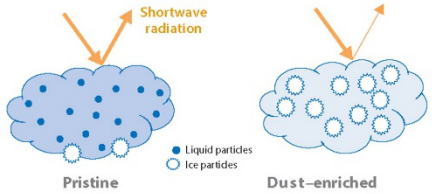

e Dust indirect effects on cirrus clouds

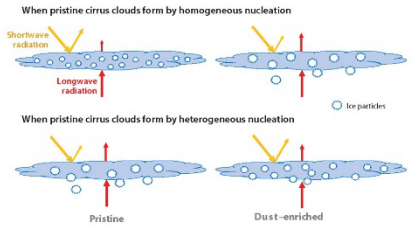

f Dust semi-direct effects on low clouds

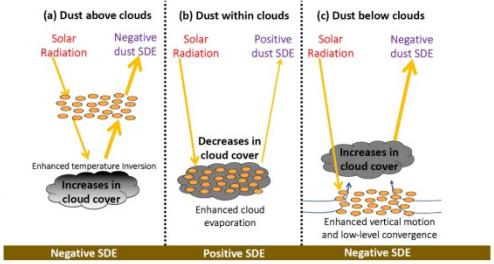

g Dust interactions with the cryosphere

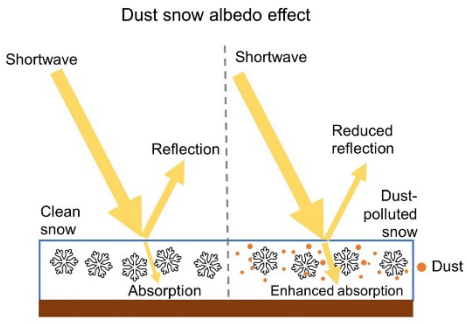

h Dust interactions with biogeochemistry

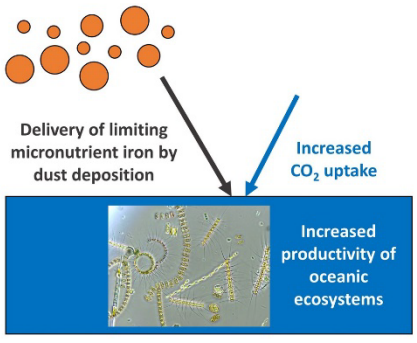

Figure 2. Mechanisms through which dust impacts climate. a | dust direct interactions with shortwave (SW) and longwave (LW) radiation. **b** | dust interactions with atmospheric chemistry and the induced perturbations to the radiative fluxes at the top-of-atmosphere exerting a warming (left) or cooling (right) effect on global climate. The brown core represents the freshly emitted insoluble dust particle and the surrounding blue area represents the acquired soluble coating through interactions with atmospheric chemistry. **c** | dust indirect effects on warm clouds occur by dust increasing cloud albedo through adding to CCN and increasing CDNC (upper branch) and by dust decreasing cloud albedo by reducing non-dust CCN through enhanced particle coagulation and adsorption of precursor gases and by dust giant CCN reducing in-cloud supersaturation (lower branch). **d** | dust indirect effects on mixed-phase clouds (MPCs), illustrated by MPC formation in pristine (left) and dust-enriched (right) environments. **e** | dust indirect effects on cirrus clouds, separated by the dominant ice crystal formation mechanism in the absence of dust. **f** | dust semi-direct effects on low clouds due to local heating generated by dust absorption, separated by location of dust relative to clouds. **g** | radiative effects of dust deposited on snow and ice, illustrated by snow reflectivity without (left) and with (right) dust deposited onto the snowpack. **h** | effect of dust on CO_2 concentrations due to interactions with ocean biogeochemistry. Yellow arrows represent SW radiation and red arrows represent LW radiation.

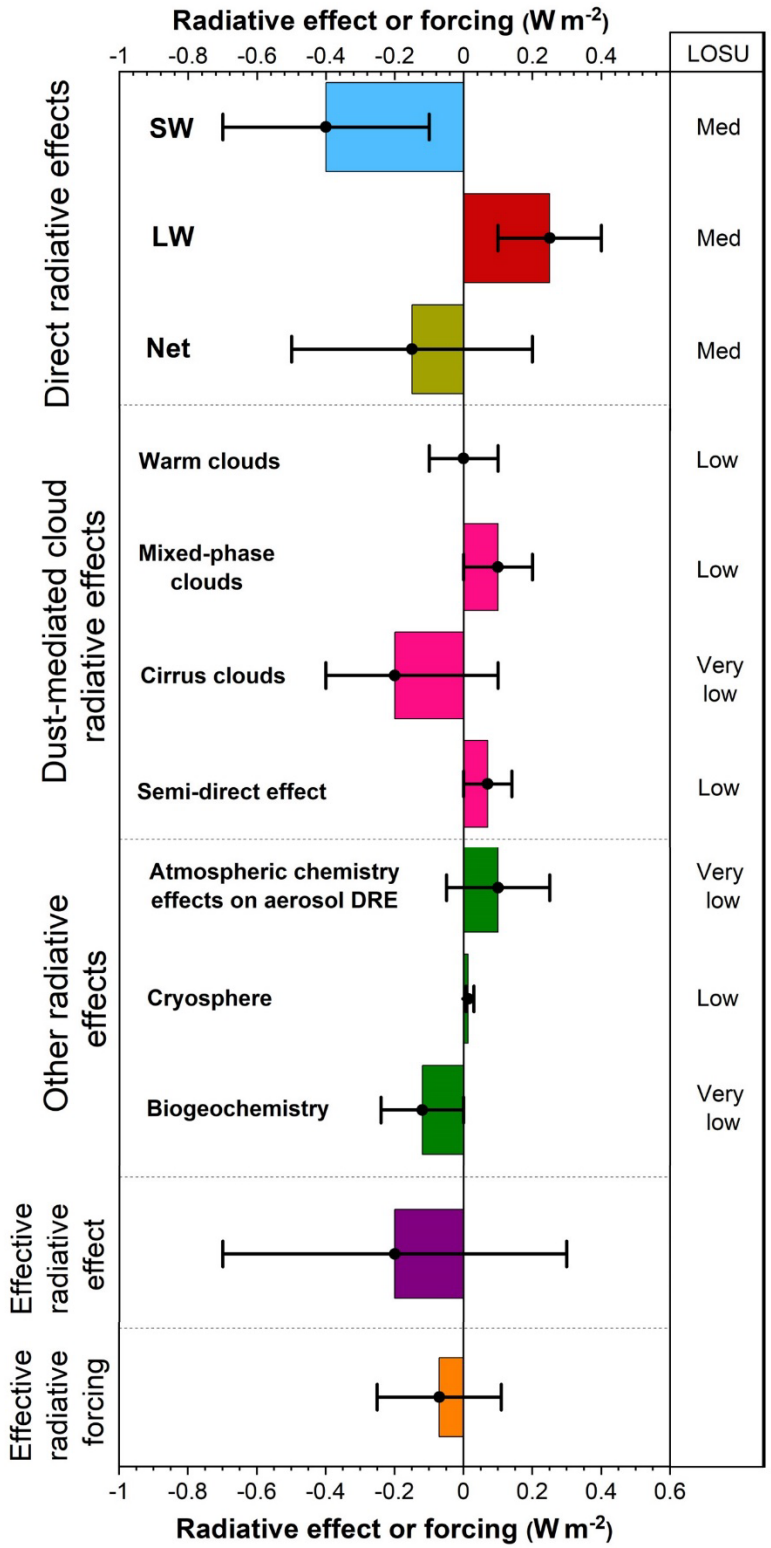

Figure 3. The global mean effective radiative effect and radiative forcing of dust at the top-of-atmosphere. Perturbations to Earth's radiation budget by dust through direct radiative effects, dust-mediated cloud radiative effects, and various other radiative effects. The sum of all radiative effects equals the dust effective radiative effect *R* (Eq. 2) and the portion of that dust effective radiative effect

that is due to the increase in dust since pre-industrial times is the effective radiative forcing $\Delta F_{\mathrm{p}\rightarrow\mathrm{m}}$ (Eq. 4). Error bars denote the 90% confidence range. The column on the right denotes the level of scientific understanding (LOSU), or confidence in the assessment of each radiative effect, following past practice[27]. The global mean dust effective radiative effect and radiative forcing of dust are uncertain in sign and magnitude, but are more likely to cool than to warm the climate.

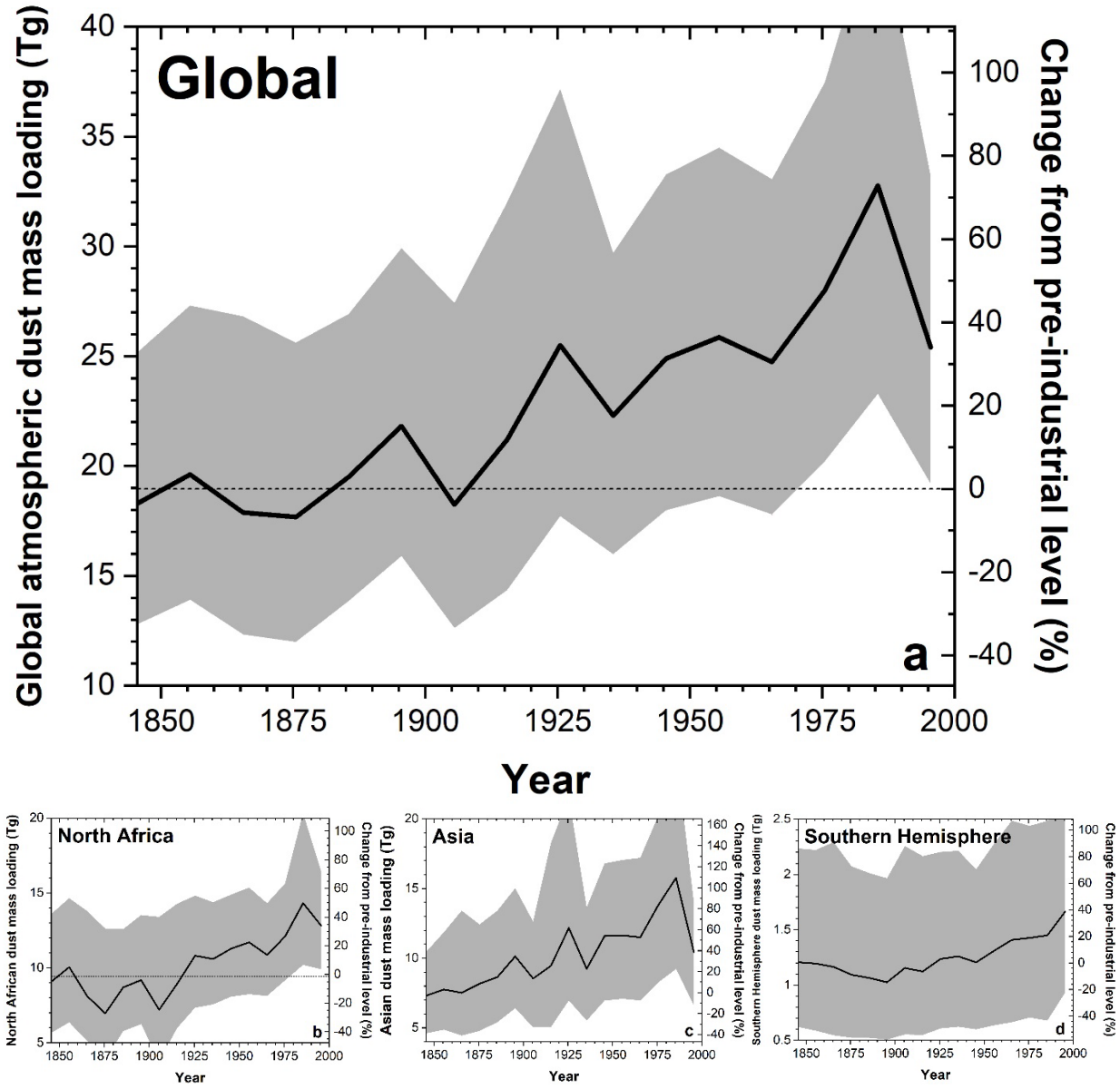

Figure 4. Atmospheric dust mass loading changes since pre-industrial times. a| Reconstructed globally integrated dust mass loading. **b**| as in a, but for loading contributed by dust from North Africa. **c**| as in a, but for loading contributed by dust from Asia. **d**| as in a, but for loading contributed by dust from the Southern Hemisphere. The solid line denotes the median dust loading estimate, the shading the 90% confidence range, and the dotted line the average pre-industrial (1841-1860) dust loading. Dust loadings were obtained by combining 19 records of dust deposition with constraints on the spatially resolved dust deposition fluxes produced by the world's main dust source regions[8,44]; see Supplement for details. Dust has increased in all three regions, translating to a 55 ± 30 % rise in global dust mass loading in modern times (1981-2000) compared to pre-industrial.

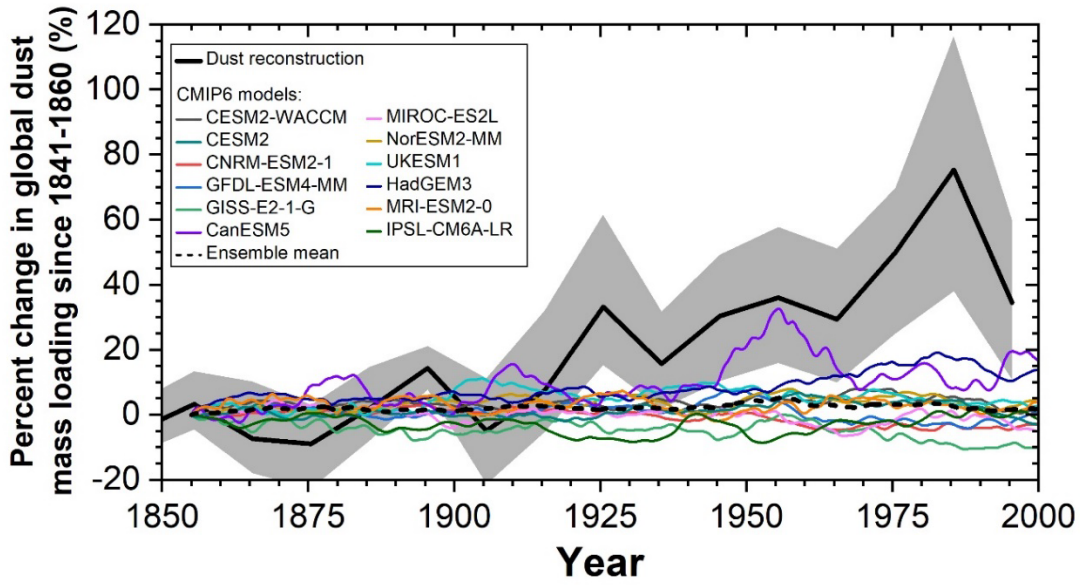

Figure 5. Climate model representations of historical changes in dust loading. Changes in global dust loading relative to the period 1841-1860 obtained from the dust reconstruction (solid black line) and simulated by 12 CMIP6 climate models with prognostic dust aerosol cycles[214] (thin colored lines). CMIP6 data are 10-year running means from historical runs[186]. Grey shading denotes the 90% confidence interval for the dust reconstruction. All models and the ensemble mean (dashed black line) fail to reproduce the large historical increase in dust loading.

Box 1. Drivers of the historical increase in dust loading. The large historical increase in dust observed in deposition records and the reconstruction of dust mass loading (Fig. 4) can be either due to human land use changes or due to natural and anthropogenic changes in climate[230].

The observational record shows that dust is highly sensitive to climate. Indeed, dust records in some regions show a variation of a factor of ~2-4 due to climate variability over the 20th century[178,180,183] and dust has increased by a factor of ~2-4 in transitions between interglacial and glacial periods[231,232]. As such, changes in aridity, vegetation cover, and wind speed due to natural climate variability could have driven (part of) the long-term increase in dust loading, as has been suggested for North Africa[178,180,233]. In addition, anthropogenic changes to climate and atmospheric composition could also have affected dust loading, both by increasing aridity and by higher CO2 concentrations fertilizing plants at desert margins[234], with the net effect on desert extent and dust emissions still unclear[235].

Human land use changes could also have increased dust emissions. The Industrial Revolution and the rise of industrialized agriculture have resulted in a dramatic increase in the area of land used by humans: the fraction of the ice-free land area used for agriculture has quadrupled from ~9% in 1850 to ~35% in 2000[236]. This large-scale conversion of wildlands to agricultural land has included many semi-arid and arid regions (Fig. 1), for which human land use changes can result in dramatic increases in dust emission[237-239]. Additionally, anthropogenic changes in water management that result in the drying of inland bodies of water might also have substantially increased dust emissions, such as has occurred for Owen's Lake in California in the early 20th century[240] and more recently for the Aral Sea in Central Asia[241,242].

Modelling has been unable to determine whether the historical increase in dust, which models have been unable to reproduce[22] (Fig. 5), has been primarily driven by climate or land use changes. Indeed, past research has diverged on the fraction of the global dust burden in the current climate emitted from anthropogenically disturbed sources, with results ranging from as little as 0% to as much as 50%[199,207,230,243-245]. Similarly, modelling results on effects of changes in climate and CO_2 concentrations on dust loading also differ, with results varying between a decrease of -20% and an increase of +60% in dust loading[199,230,235].

Although large uncertainties thus remain in how climate and land use changes have contributed to the historical increase in dust loading (Fig. 4), two observational findings suggest that anthropogenic land use change has been a key driver of the long-term increase in dust loading (Fig. 4). First, the timing of increases in dust deposition in various deposition records appears to coincide with the rise of industrialized agriculture in source regions[23]. And second, satellite observations suggest that ~25% of modern dust emissions originate from regions heavily impacted by human land use[191]. This finding implies that human land use changes have increased dust mass loading by ~33% since pre-industrial times, which accounts for the majority of the 55 ± 30% increase in dust mass loading since pre-industrial times (Fig. 4). Moreover, satellite observations indicate that the fraction of dust emitted from anthropogenically disturbed surfaces is substantially higher for Asian than for North African source regions, which is qualitatively consistent with the finding of a larger historical increase of Asian than of North African dust (Figs. 4b-d). Nonetheless, substantial additional work is needed to determine the exact causes of the historical increase in dust for each of the world's main dust source regions.

Supplementary Methods

We reconstructed atmospheric dust loading between the years 1841-2000 by combining a compilation of dust deposition records with constraints on the deposition flux produced by each of nine major source regions to each deposition site. These constraints on source-resolved deposition fluxes were obtained from the Dust Constraints from joint Observational-Modelling-Experimental analysis (DustCOMM) data set. This data set includes uncertainties on deposition fluxes that comparisons against independent data suggest are realistic[1,2].

Our approach is an extension of the methodology used in Mahowald et al.[3], who also used a compilation of dust deposition records to reconstruct dust loading. We improved upon the approach in Mahowald et al.[3] in a number of ways. First, we used almost double the number of dust deposition records (19 versus 11), including several recently published records that constrain dust from North Africa and East Asia[4-9]. These two source regions together account for ~60% of global dust loading[2] but most deposition records constraining these two regions were not available in Mahowald et al.[3]. Second, we used explicit constraints on the contributions of the different source regions to the deposition flux at each site, allowing a statistical approach that finds the most likely evolution of dust loading over time for each of nine major dust source regions[1,2]. Finally, we used a bootstrap approach with resampling to propagate errors in both deposition flux records and in the DustCOMM source region-resolved deposition fluxes[10,11].

Below, we first describe the compilation of dust deposition records, after which we describe the methodology for reconstructing dust loading.

Compilation of dust deposition records

To construct our compilation of dust deposition records, we built on the compilation of 25 deposition records obtained by Hooper and Marx[12]. Each of these records span at least 150 years of the pre-industrial to modern climate, ends after 1975, and has a time resolution of at least one data point per 10 years. Some of these records are based on measurements of dust particles in a sedimentary matrix (e.g., ice) and some are based on proxies for dust, such as the concentration of crustal elements like Mg and Ca. Measurements of the concentration of dust or a dust proxy are then converted to a dust deposition flux by calculating the mass accumulation rate of the sedimentary matrix using an age model that links the depth of the sediment to its age (e.g., Ref. [13]). We use a subset of 13 of these deposition records, all of which Hooper and Marx[12] identified as being dominated by long-range transported dust, rather than by locally generated dust (also see discussion in Mahowald et al.[3]). Note that these 13 records exclude three dust records from Antarctic ice cores that were used in Hooper and Marx[12] but that were affected by local dust emissions (WAIS[14] and Mount Erebus[15]) or that are unpublished data sets (Siple Dome). Because these 13 records included only one record dominated by North African dust[6], we added four more published deposition records dominated by North African dust, namely records from Barbados[4], the Swiss-Italian Alps[5], Corsica[7], and Cape Verde[16]. Additionally, we added deposition records from the northern Antarctic Peninsula[17] and the Colorado mountains[18], both of which were used by Mahowald et al.[3]. All deposition records used in this study are listed in Table S1.

Data from all deposition records were processed as follows. First, the data from each deposition record were linearly interpolated to obtain annual values in the period 1841-2000, after which all fluxes were normalized to the value of the median dust flux in the period 1991-2000. If the

record was missing data, either at the start or end of the 1841-2000 period, then these data points were filled in by taking the median of the 10 years most proximal to the missing data. We then took the median dust flux for each decade to reduce the substantial noise and year-to-year variability contained in some deposition records, which might be due to various factors unrelated to changes in dust emitted from large source regions (see Refs. [2,19,20] and further discussion below).

An exception on the data processing procedure above was made for the Cape Verde record of Evan & Mukhopadhyay[16]. This data set is unusual in that its accuracy was confirmed by correlation with satellite-observed aerosol optical depth data, but this data set also only spans the period 1955 – 2000. To fill in this record in the period 1841-1954, we used the mean of the normalized fluxes for the four other records that are dominated by North African dust, namely from Mauritania Canyon[6], the Bahamas[4], the Swiss-Italian Alps[5], and Corsica[7]. We then normalized the mean of those four records such that the dust flux over the period 1955-1974 equaled that of the Evan & Mukhopadhyay[16] record.

Reconstruction of dust loading since pre-industrial times

We used the compilation of dust deposition records to reconstruct the historical changes in dust loading generated by each of nine source regions. To do so, we used the DustCOMM data constraints on the relative contribution of each source region to each deposition core site in the modern climate (Fig. S1). That is, given the compilation of deposition flux timeseries, we obtained the evolution of normalized dust loading per source region that minimizes the disagreement between the deposition flux timeseries and the reconstructed dust loading. Specifically, we obtained the time evolution of dust loading generated by each source region by finding, for each decade, the values that minimizes the cost function[1]

$$\chi(t)^2 = \sum_{j=1}^{N_{\mathrm{dep}}} \left[\sum_{i=1}^{N_{\mathrm{sr}}} \lambda_i(t) \hat{f}_{i,j}^{\mathrm{cc}} - \tilde{\beta}_j(t) \right]^2 , \tag{S1}$$

where $N_{\mathrm{dep}} = 19$ is the number of deposition flux timeseries in the compilation (Table S1) and $N_{\mathrm{sr}} = 9$ is the number of source regions, which are western North Africa, eastern North Africa, the Southern Sahara and Sahel, the Middle East & Central Asia, East Asia, North America, Australia, South America, and Southern Africa (see Fig. S1 and Ref. [1]). Together, these 9 source regions account for the vast majority of natural dust emissions[1]. However, emissions from high latitudes (~2-3% of global emissions[21]) and from anthropogenic activities like industrial processes and vehicular traffic on dirt roads are not included[22]. Furthermore, $\hat{f}_{i,j}^{\mathrm{cc}}$ is the DustCOMM constraint on source region *i*'s fractional contribution to deposition site *j* in the current climate, and $\tilde{\beta}_j(t)$ is the measured deposition flux at site *j* for decade *t,* normalized by the median dust deposition flux in the period 1991-2000. Finally, $\lambda_i(t)$ is the normalized globally integrated dust loading generated by source region *i*,

$$\lambda_i(t) = \frac{L_i(t)}{L_i^{cc}}, \tag{S2}$$

where $L_i(t)$ is the dust loading generated by source region *i* in decade *t* and L_i^{cc} is the DustCOMM constraint on the dust loading generated by source region *i* in the modern climate (see Table 1 in Ref.[2]). Because the DustCOMM constraints were obtained for the years 2004-

2008, here we need to assume that dust loading in the period 1991-2000 equals that in the period 2004-2008, which introduces additional error in our results. Furthermore, Eqs. (S1) and (S2) assume that a source region's deposition flux scales linearly with its globally integrated dust loading.

Note that the solution for Eq. (S1) is over-constrained, with 19 deposition cores and only nine source regions, which helps reduce errors on $\lambda_i(t)$. Nonetheless, because deposition fluxes from the Western North Africa, Eastern North Africa, and Sahel source regions tend to be correlated, and because of a dearth of deposition records dominated by dust from the Sahel and Eastern North Africa, we cannot separately constrain the Western North Africa (i = 1), Eastern North Africa (i = 2), and Sahel (i = 3) source regions. Therefore, we grouped these three source regions into a single source region similar to the North Africa source region used in Mahowald et al.[3], meaning that we forced $\lambda_1(t) = \lambda_2(t) = \lambda_3(t)$ when solving (S1). Furthermore, we keep the Southern Africa source region (i = 9) constant (i.e., $\lambda_9(t) = 1$) because none of the deposition records are dominated by dust from this relatively minor source region (~1-2% of global dust loading[2]), making its temporal evolution under-constrained.

Measurements of deposition fluxes and DustCOMM constraints on the relative contribution of each source region both carry substantial uncertainties[2,23-25]. We propagated these uncertainties into $\lambda_i(y)$ and thus into the reconstruction of each source region's globally integrated loading using a bootstrap procedure[10,11] in which we resample the deposition sites. Specifically, we repeat the following steps (also see Ref.[1]) a large number of times (~1,000):

1. We obtain a realization of the 3D global dust cycle, including the source region-resolved deposition flux to each deposition site, per the procedure detailed in Kok et al.[1] (see especially section 2.4 in Ref. [1]). From this realization, we obtain $\hat{f}_{i,j}^{cc}$ and L_i^{cc}.
2. We randomly draw, with replacement, 19 cores from our compilation of 19 cores. As such, for each iteration, some cores will be used not at all, some only once, and some more than once. This resampling procedure propagates uncertainty due to errors in the dust deposition records and yields $\tilde{\beta}_j(y)$.
3. We use equation S1 to obtain $\lambda_i(t)$, the globally integrated normalized dust loading for each source region. To prevent unrealistic solutions from propagating into our results, for instance for when a random drawing of deposition cores in step 2 results in one or more source regions being poorly constrained, we only use an iteration's result if the change in the dust loading due to each source region is less than a factor of five (i.e., $\min\left(\frac{L_i(t)}{L_i^{cc}}\right) > 0.2$ and $\max\left(\frac{L_i(t)}{L_i^{cc}}\right) < 5$).
4. We use equation S2 to calculate $L_i(t)$ and the time evolution of the globally integrated dust loading as $L_{\mathrm{glb}}(t) = \sum_{i=1}^{N_{\mathrm{sr}}} L_i(t)$.

This approach yields a large number of realizations that represent the probability distribution of $L_i(t)$ and $L_{\mathrm{glb}}(t)$. We report the median and one standard error range of these results in Figures 4 and 5 in the main text. Additionally, we show the resulting comparisons against each of the 19 deposition cores in Fig. S2 and the reconstructed loading for each source region in Fig. S3. We also compare the dust reconstruction against long-term dust surface concentration measurements made since the 1970s at Barbados and Miami in Fig. S4. The dust reconstruction is in excellent

agreement with the Barbados record (Fig. S4a) and captures the trend in the Miami record, although it underestimates the magnitude of the peak dust loading in the 1980s there (Fig. S4b).

As discussed in more detail in Mahowald et al.[3], using deposition cores to reconstruct global dust loading requires a number of critical assumptions that could introduce large errors in the results, not all of which are quantified by our error propagation procedure. First, our methodology assumes that the spatial pattern of the dust deposition flux per source region has not changed since pre-industrial times. This is likely inaccurate, as the historical increase in dust loading suggests that new source regions have been activated over time, either by climate or human land use changes. However, the effect of this limitation on our results might be limited because variability of simulated dust emissions in even the modern climate is very large (e.g., Figure 2 in Ref.[26]) and DustCOMM draws on simulations from six different global models. Because satellite analyses indicate that ~25% of present day emissions are generated from surfaces with substantial human land use[27] it thus appears unlikely that the difference in the spatial pattern between dust emissions in the modern and pre-industrial period will be large compared to the substantial diversity in the spatial pattern of emissions that is already accounted for by DustCOMM. Second, measurements and simulations of dust deposition fluxes are subject to large experimental and representation errors[23,26,28], which could cause further errors in the reconstruction of global dust loading. Our approach of using relative changes in dust deposition over time at each deposition site addresses this concern somewhat as errors in trends of dust deposition fluxes are usually substantially lower than in absolute values[4]. Third, trends in dust fluxes at deposition sites might not reflect trends in dust emissions but instead in dust transport pathways[19] and in the precipitation that drives wet deposition[29]. However, ice core records indicate that rates of sea-salt aerosol deposition have remained approximately constant since pre-industrial times, which indicates that wet deposition rates have not changed substantially[30]. The effect of possible changes in dust transport pathways are difficult to quantify and it is possible that a trend in deposition data at a given site is due to long-term changes in dust transport pathways rather than changes in emissions. This concern about changes in transport causing spurious trends in deposition data is ameliorated somewhat by our use of deposition data from 19 deposition sites (Table 1). That is, because the bias caused by changes in transport pathways will differ for each site it constitutes a random error, the effect of which is thus reduced with more data. Also note that this random error is inherently propagated into our results by the bootstrap procedure with resampling. Fourth, trends in deposition fluxes will not be reflective of trends in major source regions if dust from a deposition site is dominated by local dust or by dust from a non-representative subsection of a major source region[29]. Errors in the classification of which deposition records are reflective of long-range transported dust from major source regions[3,12] could thus cause errors in the dust reconstruction. Also note that more deposition records could facilitate a substantially more accurate dust reconstruction because it could allow the use of smaller source regions in solving Eq. (S1); for instance, more deposition records could allow the temporal evolution of the western North Africa, eastern North Africa, and Southern Sahara and Sahel to be solved without combining these source regions. Considering these potentially substantial sources of uncertainty, the error estimates on our reconstructed global dust loading should be considered a lower bound.

Supplementary Figures and Tables

Table S1. Summary of compilation of dust deposition records.

Dust deposition site	Region	Type of record	Latitude	Longitude	Associated source(s)*	Record length	Approximate age resolution	Reference
NEGIS	Greenland	Ice core	75.62º	-35.96º	East Asia, North Africa, North America	1607 – 2005	1 year	Vallelonga et al. (2014)[31]
GISP2	Greenland	Ice core	72.6º	-38.5º	East Asia, North Africa, North America	665 – 1990	2-3 years (irregular)	Zielinski & Mershon (1997)[32]
20D	Greenland	Ice core	65.02º	-44.87º	East Asia, North Africa, North America	1767 – 1984	1 year	Kang et al. (2003)[33]
Mount Logan	Yukon, Canada	Ice core	60.58º	-140.5º	East Asia	1000 – 1998	1 year	Osterberg et al. (2008)[9]
Motianling	Great Hinggan Range, China	Peat core	47.35º	120.65º	East Asia	1860 – 2007	3-30 years (irregular)	Bao et al. (2012)[8]
Point d'Escuminac	New Brunswick, Canada	Peat core	46.92º	-65.5º	North America	1550 – 1996	4-25 years (irregular)	Kylander et al. (2009)[34]
San Juan Lakes	Colorado, USA	Lake sediment core	38º	-108º	North America	1855 - 2005	30 years	Neff et al. (2008)[18]
Dasuopo	Mount Xixiabangma, Himalaya	Ice core	28.38º	85.72º	Middle East / Central Asia	1450 – 1996	1 year	Thompson et al. (2000)[35]
Mount Everest #1	East Rongbuk Glacier, Himalaya	Ice core	28.03º	86.96º	Middle East / Central Asia	1690 - 2002	1 year	Kaspari et al. (2009)[36]
Mount Everest #2	East Rongbuk Glacier, Himalaya	Ice core	27.98º	86.92º	Middle East / Central Asia	1843 – 1997	1 year	Kang et al. (2003)[33]
Mauritania Canyon	Atlantic Ocean	Ocean sediment core	16.83º	-16.73º	North Africa	1180 BC – 2005	1-2 years	Mulitza et al. (2010)[6]
Sal Island	Cape Verde	Coral core	16.76º	-22.89º	North Africa	1955 – 2008	1 year	Evan & Mukhopadhyay (2010)[16]
Andros Island	Bahamas	Coral core	25º	-78º	North Africa	1065 – 2011	10-30 years (irregular)	Hayes et al. (2017)[4]
Colle Gnifetti	Italian Alpes	Ice core	45.94º	7.88º	North Africa	1780 – 2006	1 year	Clifford et al. (2019)[5]
Lake Bastani†	Corsica	Lake sediment core	42.07º	9.13º	North Africa	1220 BC - 2013	3-4 years	Sabatier et al. (2020)[7]; Pierre Sabatier, personal communication (2022)
Snowy Mountains	NSW, Australia	Peat core	-36.46º	148.3º	Australia	500 – 2005	2 – 10 years (irregular)	Marx et al. (2014)[37]
Law Dome	Budd Coast, East Antarctica	Ice core	-66.77º	112.8º	South America, Australia	1480 – 1996	1 year	Souney et al. (2002)[38]
Siple Station	Ellsworth land, West Antarctica	Ice core	-75.92º	-84.25º	South America, Australia	1417 – 1983	1 year	Mosley-Thompson et al. (1990)[39]

James Ross Island	Northern Antarctic Peninsula	Ice core	-64.2º	-57.7º	South America	1832 - 1991	1 year	McConnell et al. (2007)[17]

*Associated sources are based on Fig. S1.
†The data of Sabatier et al.[7] were further corrected for sediment matrix effects through centered-log-ratio (CLR) transformation (Sabatier, personal communication, 2022).

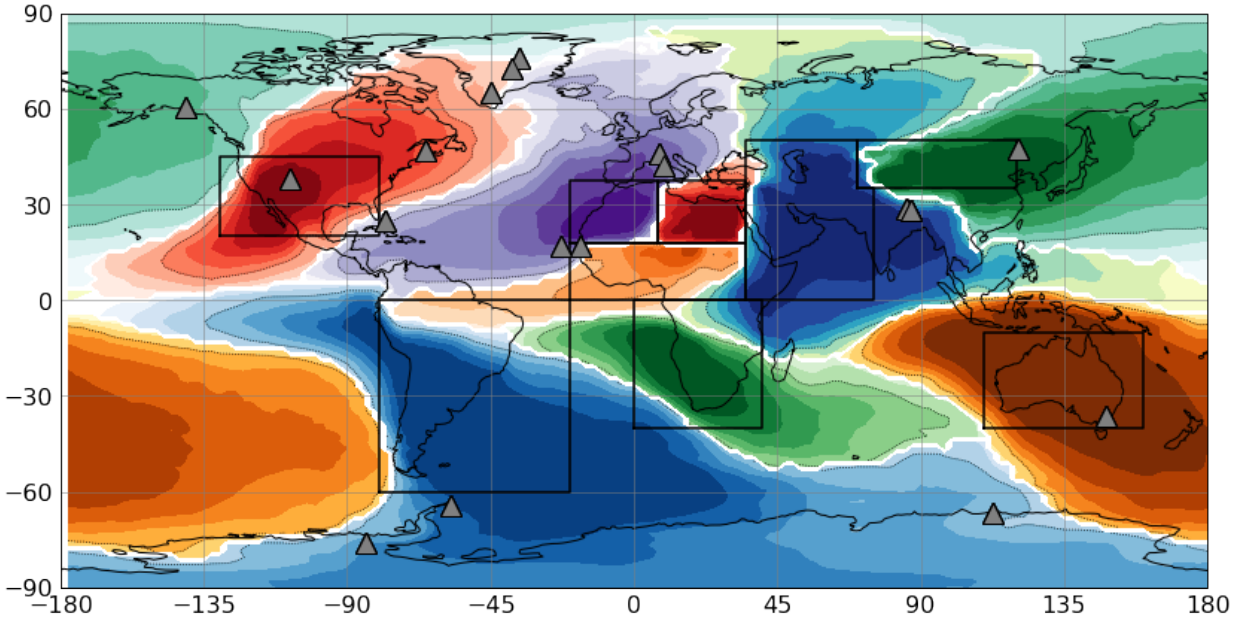

Figure S1. Map of deposition record sites and dominant dust source regions. Different colors represent the fraction of the dust deposition flux supplied by different dominant source regions, with shading decreasing in increments of 0.1 from a maximum of 1. The black boxes denote the nine major source regions (western North Africa, eastern North Africa, the Southern Sahara and Sahel, the Middle East & Central Asia, East Asia, North America, Australia, South America, Southern Africa). Gray triangles denote the locations of the 19 dust deposition records used to reconstruct dust loading since pre-industrial times. After Ref. [2].

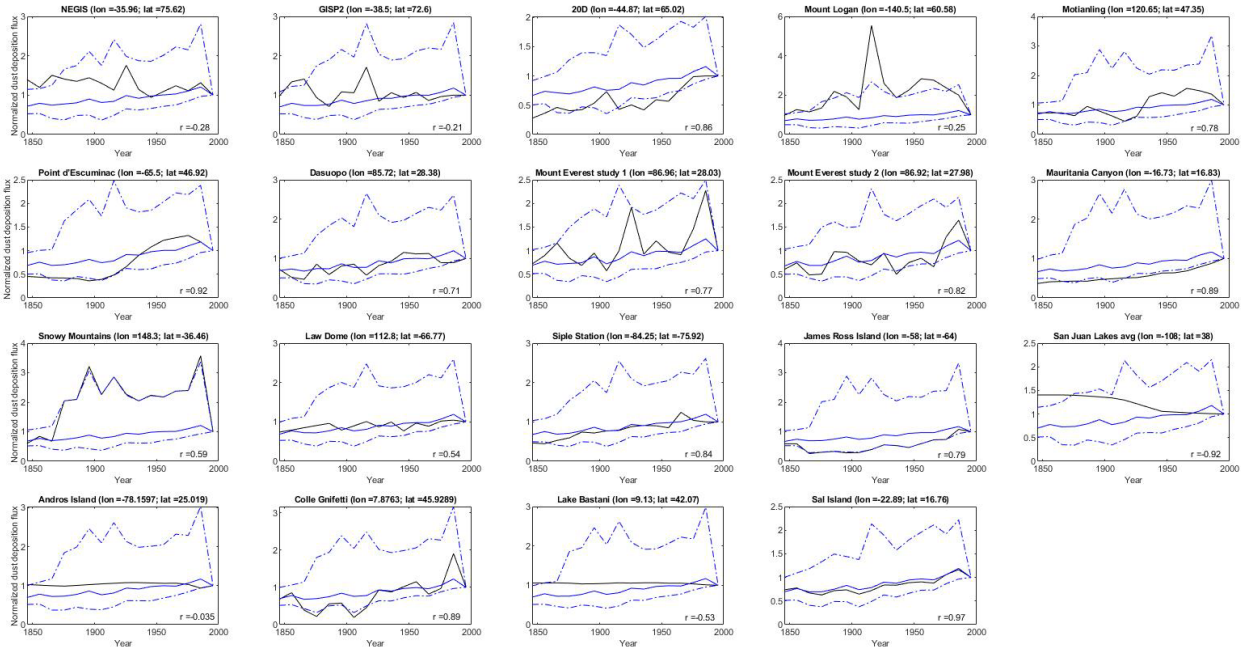

Figure S2. Comparisons between dust deposition records and reconstructed dust deposition fluxes. Shown are results for the 19 deposition records in our compilation (Table S1). The solid black line represents the measured normalized deposition fluxes (or deposition flux proxy) after data processing (see text), the solid blue line the median reconstructed normalized deposition flux, and the dash-dotted blue lines the one standard error interval on the reconstructed normalized deposition flux. Also listed is the correlation coefficient between the measured and median reconstructed normalized deposition fluxes.

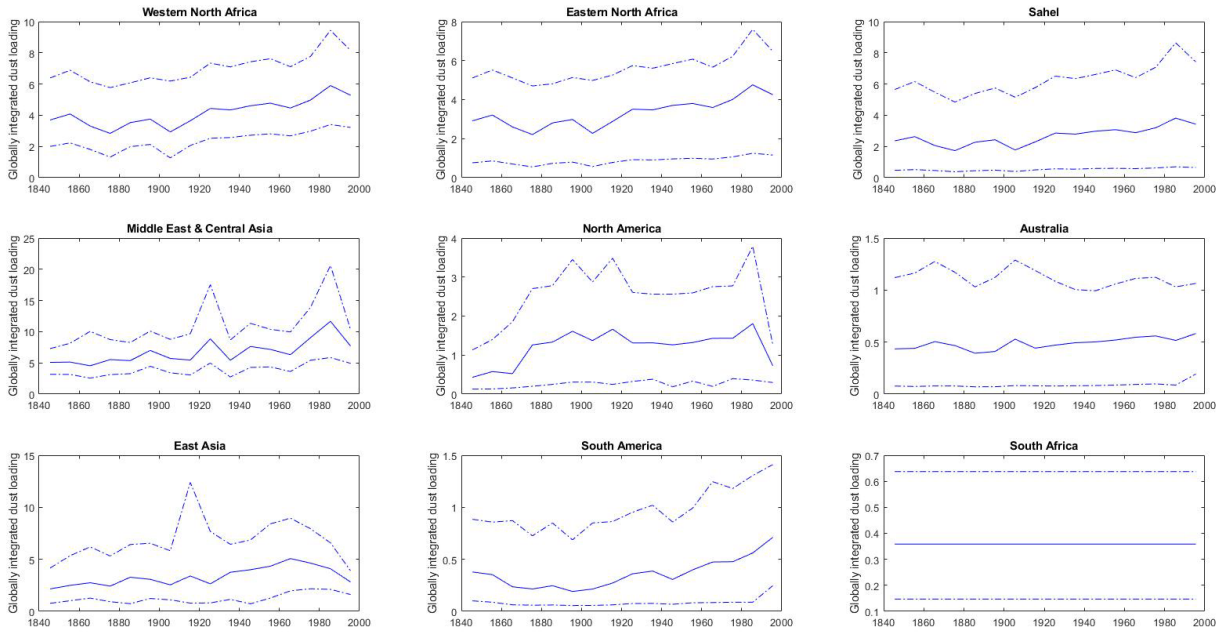

Figure S3. Reconstructed globally integrated dust loading for each source region. The solid line represents the median estimate and the dash-dotted lines the one standard error interval.

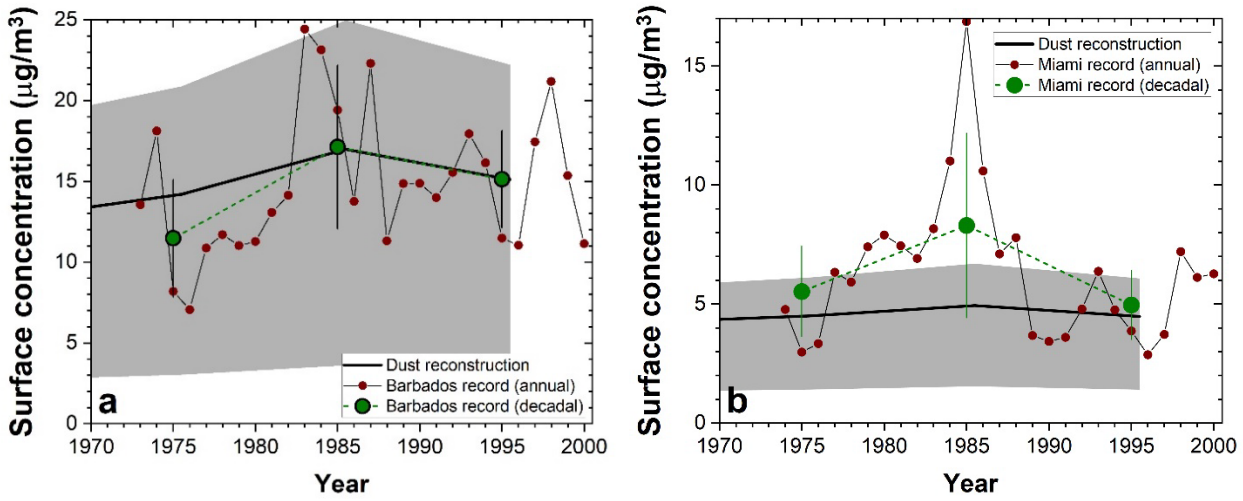

Figure S4. Comparison of dust reconstruction against long-term dust surface concentration measurements. a| Comparison against measurements at Barbados. **b**| Comparison against measurements at Miami. Small brown circles denote the measured annual average surface concentration, which was calculated from previously reported monthly average values[40]. Large green circle denote decadal averages of the annual values for a more direct comparison against the dust reconstruction. Error bars on the decadal values denote the standard deviation of the annual values. The solid black line denotes the median estimate of the reconstructed dust surface concentration and the shading denotes the 90% confidence range.

References

1 Kok, J. F. *et al.* Improved representation of the global dust cycle using observational constraints on dust properties and abundance. *Atmos. Chem. Phys.* **in press** (2021).

2 Kok, J. F. *et al.* Contribution of the world's main dust source regions to the global cycle of desert dust. *Atmos. Chem. Phys. Discuss. [preprint]* **in review** (2021). https://doi.org:10.5194/acp-2021-4

3 Mahowald, N. M. *et al.* Observed 20th century desert dust variability: impact on climate and biogeochemistry. *Atmos. Chem. Phys.* **10**, 10875-10893 (2010). https://doi.org:10.5194/acp-10-10875-2010

4 Hayes, C. T., McGee, D., Mukhopadhyay, S., Boyle, E. A. & Maloof, A. C. Helium and thorium isotope constraints on African dust transport to the Bahamas over recent millennia. *Earth and Planetary Science Letters* **457**, 385-394 (2017). https://doi.org:10.1016/j.epsl.2016.10.031

5 Clifford, H. M. *et al.* A 2000 Year Saharan Dust Event Proxy Record from an Ice Core in the European Alps. *Journal of Geophysical Research-Atmospheres* **124**, 12882-12900 (2019). https://doi.org:10.1029/2019jd030725

6 Mulitza, S. *et al.* Increase in African dust flux at the onset of commercial agriculture in the Sahel region. *Nature* **466**, 226-228 (2010). https://doi.org:10.1038/nature09213

7 Sabatier, P. *et al.* Past African dust inputs in the western Mediterranean area controlled by the complex interaction between the Intertropical Convergence Zone, the North Atlantic Oscillation, and total solar irradiance. *Clim. Past.* **16**, 283-298 (2020). https://doi.org:10.5194/cp-16-283-2020

8 Bao, K. S. *et al.* Recent atmospheric dust deposition in an ombrotrophic peat bog in Great Hinggan Mountain, Northeast China. *Science of the Total Environment* **431**, 33-45 (2012). https://doi.org:10.1016/j.scitotenv.2012.05.014
9 Osterberg, E. *et al.* Ice core record of rising lead pollution in the North Pacific atmosphere. *Geophysical Research Letters* **35** (2008). https://doi.org:10.1029/2007gl032680
10 Chernick, M. R. *Bootstrap methods : a guide for practitioners and researchers*. 400 (Wiley-Interscience, 2007).
11 Efron, B. *The jackknife, the bootstrap, and other resampling plans*. (Capital City Press, 1982).
12 Hooper, J. & Marx, S. A global doubling of dust emissions during the Anthropocene? *Glob. Planet. Change* **169**, 70-91 (2018). https://doi.org:10.1016/j.gloplacha.2018.07.003
13 Albani, S. *et al.* Twelve thousand years of dust: the Holocene global dust cycle constrained by natural archives. *Climate of the Past* **11**, 869-903 (2015). https://doi.org:10.5194/cp-11-869-2015
14 Koffman, B. G. *et al.* Centennial-scale variability of the Southern Hemisphere westerly wind belt in the eastern Pacific over the past two millennia. *Clim. Past.* **10**, 1125-1144 (2014). https://doi.org:10.5194/cp-10-1125-2014
15 Rhodes, R. H. *et al.* Little Ice Age climate and oceanic conditions of the Ross Sea, Antarctica from a coastal ice core record. *Clim. Past.* **8**, 1223-1238 (2012). https://doi.org:10.5194/cp-8-1223-2012
16 Evan, A. T. & Mukhopadhyay, S. African Dust over the Northern Tropical Atlantic: 1955-2008. *Journal of Applied Meteorology and Climatology* **49**, 2213-2229 (2010). https://doi.org:10.1175/2010jamc2485.1
17 McConnell, J. R., Aristarain, A. J., Banta, J. R., Edwards, P. R. & Simoes, J. C. 20th-Century doubling in dust archived in an Antarctic Peninsula ice core parallels climate change and desertification in South America. *Proc. Natl. Acad. Sci. U. S. A.* **104**, 5743-5748 (2007). https://doi.org:10.1073/pnas.0607657104
18 Neff, J. C. *et al.* Increasing eolian dust deposition in the western United States linked to human activity. *Nature Geoscience* **1**, 189-195 (2008). https://doi.org:10.1038/ngeo133
19 Smith, M. B. *et al.* Sensitivity of the interannual variability of mineral aerosol simulations to meteorological forcing dataset. *Atmospheric Chemistry and Physics* **17**, 3253-3278 (2017). https://doi.org:10.5194/acp-17-3253-2017
20 Albani, S. *et al.* Paleodust variability since the Last Glacial Maximum and implications for iron inputs to the ocean. *Geophysical Research Letters* **43**, 3944-3954 (2016). https://doi.org:10.1002/2016gl067911
21 Bullard, J. E. *et al.* High-latitude dust in the Earth system. *Reviews of Geophysics* **54**, 447-485 (2016). https://doi.org:10.1002/2016rg000518
22 Kok, J. F. *et al.* Contribution of the world's main dust source regions to the global cycle of desert dust. *Atmospheric Chemistry and Physics* **21**, 8169-8193 (2021). https://doi.org:10.5194/acp-21-8169-2021
23 Cakmur, R. V. *et al.* Constraining the magnitude of the global dust cycle by minimizing the difference between a model and observations. *Journal of Geophysical Research-Atmospheres* **111**, D06207 (2006). https://doi.org:10.1029/2005jd005791
24 Stanelle, T., Bey, I., Raddatz, T., Reick, C. & Tegen, I. Anthropogenically induced changes in twentieth century mineral dust burden and the associated impact on radiative

forcing. *Journal of Geophysical Research-Atmospheres* **119**, 13526-13546 (2014). https://doi.org:10.1002/2014jd022062

25 Avila, A., QueraltMitjans, I. & Alarcon, M. Mineralogical composition of African dust delivered by red rains over northeastern Spain. *Journal of Geophysical Research-Atmospheres* **102**, 21977-21996 (1997). https://doi.org:10.1029/97jd00485

26 Wu, C. C., Lin, Z. & Liu, X. The global dust cycle and uncertainty in CMIP5 (Coupled Model Intercomparison Project phase 5) models. *Atmospheric Chemistry and Physics* **20**, 10401-10425 (2020). https://doi.org:10.5194/acp-20-10401-2020

27 Ginoux, P., Prospero, J. M., Gill, T. E., Hsu, N. C. & Zhao, M. Global-scale attribution of anthropogenic and natural dust sources and their emission rates based on MODIS Deep Blue aerosol products. *Reviews of Geophysics* **50**, Rg3005 (2012). https://doi.org:10.1029/2012rg000388

28 Yu, H. B. *et al.* Estimates of African Dust Deposition Along the Trans-Atlantic Transit Using the Decadelong Record of Aerosol Measurements from CALIOP, MODIS, MISR, and IASI. *Journal of Geophysical Research-Atmospheres* **124**, 7975-7996 (2019). https://doi.org:10.1029/2019jd030574

29 Mahowald, N., Albani, S., Engelstaedter, S., Winckler, G. & Goman, M. Model insight into glacial-interglacial paleodust records. *Quat. Sci. Rev.* **30**, 832-854 (2011). https://doi.org:10.1016/j.quascirev.2010.09.007

30 Carslaw, K. S. *et al.* Aerosols in the Pre-industrial Atmosphere. *Current Climate Change Reports* **3**, 1-15 (2017). https://doi.org:10.1007/s40641-017-0061-2

31 Vallelonga, P. *et al.* Initial results from geophysical surveys and shallow coring of the Northeast Greenland Ice Stream (NEGIS). *Cryosphere* **8**, 1275-1287 (2014). https://doi.org:10.5194/tc-8-1275-2014

32 Zielinski, G. A. & Mershon, G. R. Paleoenvironmental implications of the insoluble microparticle record in the GISP2 (Greenland) ice core during the rapidly changing climate of the Pleistocene-Holocene transition. *Geol. Soc. Am. Bull.* **109**, 547-559 (1997). https://doi.org:10.1130/0016-7606(1997)109<0547:piotim>2.3.co;2

33 Kang, S. C. *et al.* Dust records from three ice cores: relationships to spring atmospheric circulation over the Northern Hemisphere. *Atmos. Environ.* **37**, 4823-4835 (2003). https://doi.org:10.1016/j.atmosenv.2003.08.010

34 Kylander, M. E., Weiss, D. J. & Kober, B. Two high resolution terrestrial records of atmospheric Pb deposition from New Brunswick, Canada, and Loch Laxford, Scotland. *Science of the Total Environment* **407**, 1644-1657 (2009). https://doi.org:10.1016/j.scitotenv.2008.10.036

35 Thompson, L. G. *et al.* A high-resolution millennial record of the South Asian Monsoon from Himalayan ice cores. *Science* **289**, 1916-1919 (2000). https://doi.org:10.1126/science.289.5486.1916

36 Kaspari, S. *et al.* A High-Resolution Record of Atmospheric Dust Composition and Variability since AD 1650 from a Mount Everest Ice Core. *Journal of Climate* **22**, 3910-3925 (2009). https://doi.org:10.1175/2009jcli2518.1

37 Marx, S. K. *et al.* Unprecedented wind erosion and perturbation of surface geochemistry marks the Anthropocene in Australia. *Journal of Geophysical Research-Earth Surface* **119**, 45-61 (2014). https://doi.org:10.1002/2013jf002948

38 Souney, J. M. *et al.* A 700-year record of atmospheric circulation developed from the Law Dome ice core, East Antarctica. *Journal of Geophysical Research-Atmospheres* **107** (2002). https://doi.org:10.1029/2002jd002104

39 Mosley-Thompson, E., Thompson, L. G., Grootes, P. & Gundestrup, N. Little ice age (neoglacial) paleoenvironmental conditions at siple station, Antarctica. *J. Glaciol.* **14**, 199-204 (1990).

40 Zuidema, P. *et al.* Is Summer African Dust Arriving Earlier to Barbados? The Updated Long-Term In Situ Dust Mass Concentration Time Series from Ragged Point, Barbados, and Miami, Florida. *Bulletin of the American Meteorological Society* **100**, 1981-1986 (2019). https://doi.org:10.1175/bams-d-18-0083.1